The effect of aryl hydrocarbon receptor inhibition or knockout on the proliferation and migration of human breast cancer cells

Ninni Elise Olafsen

Clinical nutrition

60 credits

Department of Nutrition

Institute of Basic Medical Sciences

Faculty of Medicine

May 2021

2021

The effect of aryl hydrocarbon receptor inhibition or knockout on the proliferation and migration of human breast cancer cells

Ninni Elise Olafsen

http://www.duo.uio.no/

Print: Reprosentralen, University of Oslo

II

Acknowledgements

This master's thesis was conducted at the Department of Nutrition, Faculty of Medicine at the University of Oslo, from August 2020 to May 2021.

Working with this thesis has been challenging at times. However, assistance and support have never been far away. For this I would like to thank a number of people, first and foremost, my supervisor professor Jason Matthews. Thank you for the guidance and constructive feedback throughout the year. I am also grateful that you have trusted me enough to let me contribute to two of the papers published by the lab group during this year.

I would also like to thank laboratory engineer Solveig Pettersen, PhD student Marit Rasmussen and PhD student Karoline Alvik for sharing your expertise, helping me out when needed, and always answering my questions, no matter how small they might have been.

I would like to thank the class of spring 21 for the supportive and good learning environment, and all the friends I have made as a student at the University of Oslo, for all the fun and exciting years.

Last but not least, a special thanks to my family and to my friend Silje Tiana Moen for always being there for me. This would simply not have been possible without your support, and I am ever grateful.

Oslo, May 2021

Ninni Elise Olafsen

Abstract

Introduction: Breast cancer is a devastating disease and the leading cause of cancer-related deaths among women. Despite clinical successes for the treatment of many forms of breast cancer, many patients experience side effects, there is increased therapeutic resistance and there are no successful targeted therapies against triple-negative breast cancer (TNBC). Therefore, there is an urgent need for development of new treatment options. The ligand activated transcription factor aryl hydrocarbon receptor (AHR) has been proposed as a potential target for breast cancer treatment. However, the effect of targeting and inhibiting AHR has not been fully elucidated. AHR regulates xenobiotic metabolism, cell cycle progression, cell homeostasis, inflammation and tumorigenesis, and many of its ligands exhibit anti-cancer properties. The dietary AHR agonist, 3,3'-diindolylmethane (DIM), and dietary AHR antagonist, resveratrol (RES), are reported to inhibit tumor growth and progression, but whether these actions require AHR is unclear.

Aims: The aim of the current thesis was to examine the effect of AHR loss or its inhibition on the proliferative and migratory properties of estrogen receptor positive (ER^+) and TNBC cells.

Methods: AHR^{ko} cell lines of ER^+ MCF7 cells and TNBC MDA-MB-231 and MDA-MB-468 cells were generated by zinc finger nuclease and CRISPR/Cas9 technology. RT-qPCR and EROD assays were performed to determine *CYP1A1* mRNA levels and activity. Cell proliferation was measured by a CellTiter-Glo assay, and migration was measured by a scratch assay.

Results: AHR knockout reduced proliferation of MCF7 cells, but had no effect on MDA-MB-231 cell proliferation. MDA-MB-231 AHR^{ko} cells migrated significantly more than the corresponding wildtype (WT) cells. DIM reduced proliferation of MDA-MB-231 AHR^{ko} cells, and inhibited migration of both MDA-MB-231 WT and MDA-MB-231 AHR^{ko} cells. The anti-migratory effect was abolished by co-treatment with RES. RES reduced proliferation in MCF7 AHR^{ko} cells, and MDA-MB-231 WT and MDA-MB-231 AHR^{ko} cells. The anti-proliferative effect was increased upon co-treatment with DIM and RES compared with either ligand alone in all cell lines.

Conclusion: The anti-tumor effect of AHR depended on the cell type investigated and differed between the ER^+ and the TNBC cell lines. The effect of DIM and RES on proliferation and migration were independent of AHR, suggesting other regulatory mechanisms are involved.

Contents

List of tables

List of figures

List of appendix

Abbreviations

ADP	Adenosine-di-phosphate
AHH	Aryl hydrocarbon hydroxylase
AHR	Aryl hydrocarbon receptor
AHRE	Aryl hydrocarbon response element
AHRR	Aryl hydrocarbon receptor repressor
ARNT	Aryl hydrocarbon receptor nuclear translocator
B[*a*]P	Benzo-[*a*]-pyrene
bHLH	Basic helix-loop-helix
bp	Base pair
BRCA1	Breast cancer gene 1
CCND1	Cyclin D1
Cdc2	Cell-division cycle gene 2
CDK4	Cyclin-dependent kinase 4
cDNA	Complementary DNA
CRISPR/Cas	Clustered regularly interspaced short palindromic repeats (CRISPR)-CRISPR-associated protein
CYP1A1	Cytochrome P450 1A1
CYP1B1	Cytochrome P450 1B1
CYP450	Cytochrome P450
DIM	3,3'-diindolylmethane
DMEM	Dulbecco's modified eagle medium
DMSO	Dimethyl sulfoxide
DRE	Dioxin response element
E2	17β-estradiol
EMT	Epithelial-mesenchymal transition
ER	Estrogen receptor
ER$^-$	Estrogen α negative
ER$^+$	Estrogen α positive
ERE	Estrogen response element
EROD	7-ethoxyresorufin-O-deethylase
ETX	7-ethoxyresorufin
FBS	Fetal bovine serum

gDNA	Genomic DNA
HDR	Homology-directed repair
HER2	Human epidermal growth factor receptor 2
HSP90	Heat shock protein 90
I3C	Indole-3-carbinol
ICZ	5,11-dihydroindolo-[3,2-*b*]carbazole
IDO1	Indoleamine 2,3-dioxygenase 1
IHC	Immunohistochemical
KYN	Kynurenine
MMP	Matrix metalloproteinase
NFAT	Nuclear factor of activated T cells
NHEJ	Non-homologous end joining
p23	Prostaglandin E synthase 3
PAM	Protospacer adjacent motif
PAS	Period-Aryl hydrocarbon receptor nuclear translocator-Single-minded
Plk	Polo-like kinase
PR	Progesterone receptor
PX459	pSpCas9(BB)-2A-Puro
RB1	Retinoblastoma protein
RBN-2397	Ribon-2397
RES	Resveratrol
RT-qPCR	Reverse transcription-quantitative Polymerase Chain Reaction
SEM	Standard deviation of the mean
sgRNA	Single-guide RNA
SLUG	SNAI2
SMAD	Small mothers against decapentaplegic
SNAIL	SNAI1
Sp	Streptococcus pyogenes
TALEN	Transcription activator-like effector nuclease
TCDD	2,3,7,8-tetrachlorodibenzo-*para*-dioxin
TIPARP	TCDD-inducible poly ADP-ribose polymerase
TNBC	Triple negative breast cancer

XAP2	X-associated protein 2
XRE	Xenobiotic response element
ZEB	Z-finger E-box binding homeobox
ZFN	Zinc-finger nuclease

1 Introduction

1.1 Breast cancer

Breast cancer has surpassed lung cancer as the most prevalent cancer worldwide, and is the leading cause of cancer related deaths among women (1, 2). It is a heterogeneous disease, and its severity depends on the genetic traits of the tumors and whether tumors are localized or have metastasized to other tissues. Breast cancer can be categorized in different ways; however, this thesis will focus on the genetic qualities of the cancer cells and the immunohistochemical markers.

Three proteins determine which subtype the specific breast cancer falls into, and which treatment would be effective. These include estrogen receptor (ER), progesterone receptor (PR), and human epidermal growth factor receptor 2 (HER2) (3). ER and PR are hormone receptors. There are two subtypes of ERs, ERα and ERβ, and two subtypes of PRs, PR-A and PR-B. Of the hormone receptors, ERα is the most important in terms of breast cancer classification. Breast cancers can be ERα positive (ER^+) or ERα negative (ER^-), with approximately 70% of all breast cancers being ER^+. These cancers generally have a better prognosis and higher 5-year survival rate compared with other breast cancer subtypes (3). This is due to effective therapeutic agents, such as tamoxifen, which specifically inhibit ERα signaling in breast cancer (3, 4).

ER^+ breast cancer can further be divided into the subtypes Luminal A or Luminal B, depending on their expression level of HER2 (Table 1). Luminal A tumors do not express HER2, while Luminal B tumors do. Cell lines are important tools to investigate the properties of the different breast cancer subtypes. Examples of Luminal A cell lines are MCF7 and T-47D cells, while BT474 and ZR-75 are Luminal B cell lines. Another breast cancer subtype is the HER2-positive breast cancer. This subtype overexpresses HER2, but do not express ER or PR. HER2-positive breast cancer represents about 15-20% of all breast cancers (3, 5). They have a slightly poorer prognosis than Luminal A and Luminal B. Commonly used HER2-positive cell lines include SKBR3 and MDA-MB-453 cells. Lastly, triple-negative breast cancers (TNBCs) are a breast cancer subtype that do not express ER, PR or HER2, and is further divided into mesenchymal- or basal-like cancer. TNBCs represent about 15-20% of all breast cancers and have the poorest prognosis (3). Examples of TNBC cell lines are MDA-MB-231 cells, which are mesenchymal-like, and MDA-MB-468 cells, which are basal-like. In the current thesis, the Luminal A cell line MCF7 and the TNBC cell lines MDA-MB-231 and MDA-MB-468 were used.

Table 1. Immunohistochemical characteristics of the different breast cancer subtypes. Cell lines that are highlighted in bold font were used in this thesis. ER: estrogen receptor; PR: progesterone receptor; HER2: human epidermal growth factor receptor 2

Breast cancer subtypes	**Characteristics**			**Cell lines**
	ER	**PR**	**HER2**	
Luminal A	+	+/-	-	**MCF7**, T-47D
Luminal B	+	+/-	+	BT474, ZR-75
HER2-positive	-	-	+	SKBR3, MDA-MB-453
Triple-negative	-	-	-	**MDA-MB-231**, **MDA-MB-468**

1.1.1 Role of ER in breast cancer

ERs, ERα or ERβ, are ligand-dependent transcription factors, which are activated by endogenous estrogens, including estrone, 17β-estradiol (E2) and estriol, as well as numerous exogenous and dietary compounds including plant-based estrogens, referred to as phytoestrogens. ERα levels are elevated in ER^+ breast cancer and it is considered a driver of hormone-dependent tumor growth (6). Upon ligand activation, ERα or ERβ homodimerize and bind to estrogen response elements (EREs) in the promotor region of target genes (6, 7). Activation of ERα results in increased cancer cell proliferation (6), while ERβ has diverse effects on breast cancer development, and its exact role in mammary tumorigenesis remains to be determined (8).

1.1.2 Breast cancer treatment

There are many different therapeutic approaches to treat breast cancer. Choosing the best treatment option depends on the breast cancer subtype, the breast cancer stage, the general health of the patient, and whether the patient is undergoing menopause (9). Surgery is usually the first treatment step. This can be either breast-conserving surgery, where only the tumor is removed, or mastectomy, where the whole breast is removed. A double mastectomy removes both breasts. If the cancer has metastasized, it will typically first reach the lymph nodes under the arm, in which case they will be removed by surgery. Surgery is usually followed by either radiotherapy or chemotherapy to kill any remaining cancer cells. Radiotherapy uses controlled doses of radiation to kill cancer cells and is either applied to a local area of the breast or the whole breast wall, which depends on what type of surgery was performed. Chemotherapy uses cytotoxic drugs to kill cancer cells and can be used in combination with surgery. However, both

radiotherapy and chemotherapy have several side effects, including fatigue, irritation of the skin, infections, sore mouth and loss of appetite (9).

ER^+ breast cancer can be treated with selective estrogen receptor modulators like tamoxifen (6, 9), which inhibits ERα in breast tissue, thereby preventing estrogen mediated proliferation. Tamoxifen is the most commonly used drug to treat ER^+ breast cancer, and it is also used preventatively for high-risk patients (10, 11). However, a side effect of prolonged use of tamoxifen is increased risk of endometrial cancer due to its estrogen activity in the uterus (12). If a patient has experienced menopause, they may be offered an aromatase inhibitor. Aromatase is an enzyme produced in the ovaries that induce estrogen production (6). An aromatase inhibitor blocks aromatase, resulting in decreased levels of estrogen, preventing the growth of hormone-dependent breast cancer (6). If a patient has not yet experienced menopause, ovarian oblation or suppression may be an option, in which case the ovaries permanently or periodically stop producing estrogen (9).

Targeted therapies are another approach where trastuzumab (Herceptin) is the most common. This drug targets HER2 and is consequently effective against HER2-positive breast cancers. Trastuzumab blocks the effect of HER2, and indirectly encourages the immune system to attack the cancer cells (13). Unfortunately, trastuzumab has many side effects such as increased risk of infections, diarrhea, abdominal pain, weight loss, tremors, dizziness, altered blood pressure, heart failure and declined left ventricular ejection fraction (14-16).

In addition to potential side effects of the different treatment options, there is a possibility that cancer cells will develop resistance to the therapy, which is often observed after prolonged tamoxifen treatment (11, 13, 17). Several studies and clinical trials examine alternative approaches and targeting therapies to overcome therapy-resistant cancer. In addition, TNBCs lack all three receptors and are the most aggressive breast cancer subtype. Patients with TNBC have the poorest prognosis, which is mainly due to a lack of effective therapeutic options. Thus, new treatment alternatives are urgently needed. One protein that has recently gained attention as a potential therapeutic target is the aryl hydrocarbon receptor (AHR).

1.2 Aryl hydrocarbon receptor (AHR)

AHR is a ligand activated transcription factor and a member of the basic helix-loop-helix period circadian protein-aryl hydrocarbon receptor nuclear translocator-single minded (PER-ARNT-SIM, PAS) (bHLH-PAS) family of transcription factors (Figure 1). The *AHR* gene is located on chromosome 7 band p21→p15 (18), and consists of 12 exons, with a theoretical protein mass of ~96 kDa (19). The protein is highly conserved across vertebrate species, suggesting an important role in cell homeostasis and metabolism (20). AHR is expressed in various human tissues, with high mRNA levels in the liver, lung and placenta, and lower levels in skeletal muscle, brain and kidney (21). AHR has an important role in xenobiotic metabolism, although it also directly or indirectly regulates genes involved in glucose metabolism, lipid and cholesterol synthesis, the circadian rhythm and protein transport (22). *Ahr*-null mice have smaller livers, decreased body weight and reduced fertility (19).

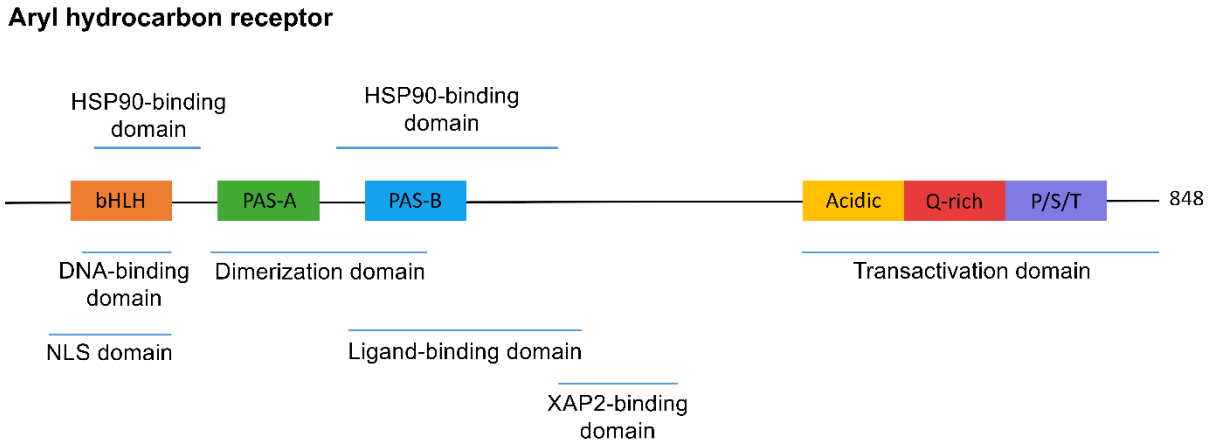

Figure 1. Schematic of the AHR protein and its functional domains. The N-terminal region contains the bHLH domain and PAS domains, which are responsible for nuclear localization (NLS domain), DNA-binding, heterodimerization and binding to the HSP90 dimer. The C-terminal region contains the transactivation domain (TAD) consisting of acidic, glutamine-rich and proline/serine/threonine-rich subdomains. bHLH: basic helix-loop-helix; PAS-A: PER-ARNT-SIM-A; PAS-B: PER-ARNT-SIM-B; Q-rich: glutamine-rich; P/S/T: proline/serine/threonine rich; HSP90: heat shock protein 90; NLS: nuclear localization signal; XAP2: X-associated protein 2.

AHR was initially discovered as the mediator of the effect of 2,3,7,8-tetrachlorodibenzo-*para*-dioxin (TCDD, dioxin) in hepatic cells of C57BL/6J mice (23). TCDD is a highly toxic compound, and is classified as a group I carcinogen by the International Agency for Research on Cancer (24). TCDD is slowly metabolized to more hydrophilic compounds and excreted;

however, the half-life of TCDD is approximately 10 years in humans because it accumulates and is stored in adipose tissue. Hence, TCDD induces a sustained hyperactivation of AHR, and a multitude of toxicological outcomes (25). AHR can be activated by a wide range of structurally diverse ligands, from both exogenous and endogenous sources. TCDD remains the most potent and stable AHR agonist, and serves as a positive control for studying the mechanisms of AHR activation in cells (26). Due to its role in TCDD toxicity, AHR's potential as a therapeutic target has been largely disregarded. However, AHR is now recognized as an essential homeostatic gatekeeper that integrates dietary, environmental, microbial and endogenous ligand signals to modulate immune cell homeostasis, inflammation and tumorigenesis in humans (27).

1.3 Mechanism of AHR

Inactive AHR is located in the cytosol of the cell in a multiprotein complex consisting of a heat shock protein 90 (HSP90) dimer, and the co-chaperones prostaglandin E synthase 3 (p23) and immunophilin-like protein hepatitis B virus X-associated protein 2 (XAP2, also known as AHR-interacting protein, AIP) (25, 28, 29). Upon binding of an AHR agonist to the PAS-B domain of the protein, the AHR complex translocates from the cytosol to the nucleus (Figure 2). The aryl hydrocarbon receptor nuclear translocator (ARNT) binds to AHR and mediates the dissociation of HSP90, p23 and XAP2. ARNT is also a member of the bHLH-PAS family, and the heterodimerization involves the HLH and PAS domains of the two proteins (30). Through the basic domain, the AHR-ARNT heterodimer binds to aryl hydrocarbon response elements (AHREs; dioxin response elements: DREs; xenobiotic response elements: XREs) that contain the core DNA sequence 5´-TNGCGTG-3´ in the regulatory regions of its target genes. After the AHR-ARNT dimer bind to an AHRE, the chromatin structure is altered and there is an increase in promoter accessibility through other co-activators (31). Finally, the general transcriptional machinery and co-regulatory proteins are recruited to the promotor region, resulting in increased transcription of a wide variety of target genes (Figure 2) (25, 30).

As with all transcription activators, it is essential to be able to regulate the activity of AHR. There are three mechanisms that inhibit the canonical AHR pathway, and subsequently transcription activation. The first mechanism is metabolism and inactivation of AHR ligands due to increased levels of metabolizing enzymes like Cytochrome P450 1A1 (CYP1A1) and CYP1B1. The second mechanism is ligand-induced proteolytic degradation of AHR by the ubiquitin-mediated proteasomal degradation system (32). The third mechanism is repression of

AHR by inhibitory proteins. These inhibitory proteins include the aryl hydrocarbon receptor repressor (AHRR) and TCDD-inducible poly ADP-ribose polymerase (TIPARP, PARP7, ARTD14) (Figure 2). Both AHRR and TIPARP are AHR target genes, and they suppress AHR activity through a negative feedback loop. AHRR functions by competitive binding to ARNT, thereby inhibiting its heterodimerization with AHR (33). TIPARP on the other hand, mono-ADP-ribosylates AHR, repressing its activity and promoting its degradation (Figure 2) (34, 35).

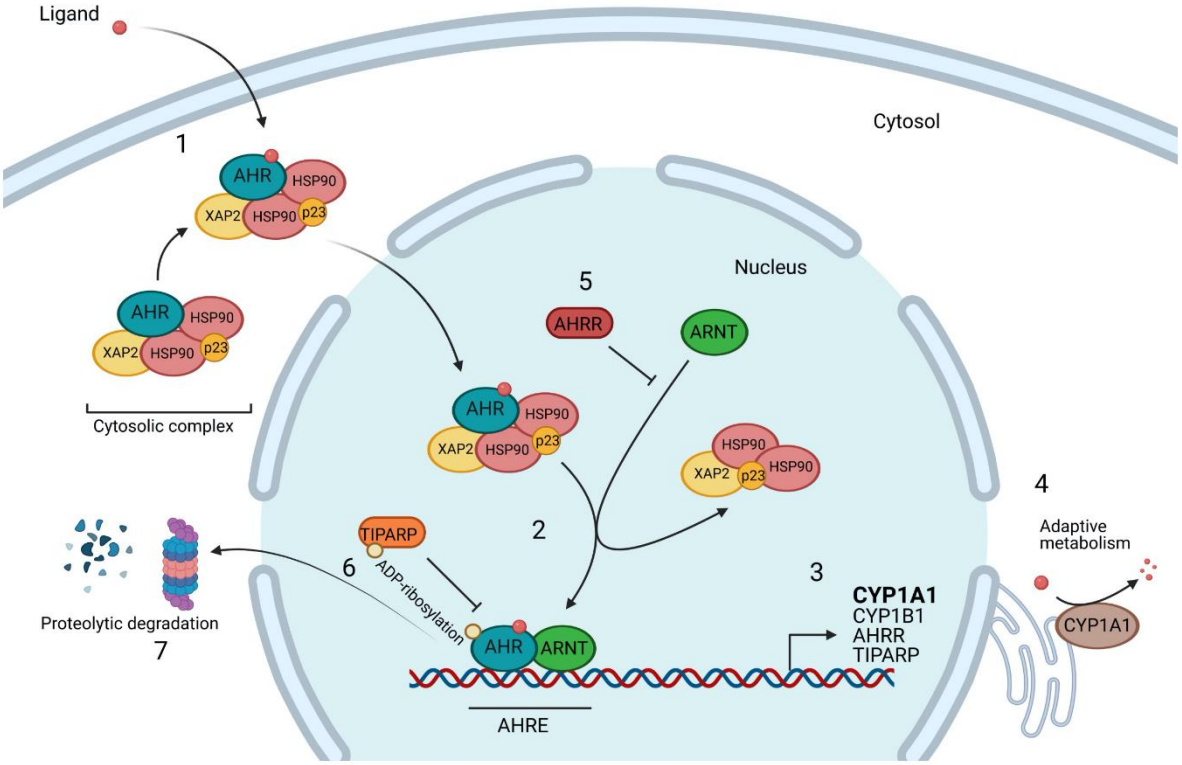

Figure 2. The canonical AHR pathway. 1 AHR is located in the nucleus in a cytosolic complex with a HSP90 dimer, p23 and XAP2. Upon ligand binding, the cytosolic complex translocates to the nucleus. **2** ARNT heterodimerizes with the ligand-activated AHR resulting in dissociation of the cytosolic complex and binding of the AHR-ARNT heterodimer to AHRE. **3** Transcription of AHR target genes are activated. **4** AHR ligands are metabolized by CYP450 enzymes like CYP1A1, an AHR target gene. **5** AHRR inhibits AHR activity by competitive binding to ARNT. **6** TIPARP mono-ADP-ribosylates AHR thereby repressing AHR activity. **7** AHR is exported to the cytosol where it is ubiquitinated and proteolytically degraded. AHR: aryl hydrocarbon receptor; HSP90: heat shock protein 90; XAP2: X-associated protein 2; p23: prostaglandin E synthase 3; ARNT: aryl hydrocarbon receptor nuclear translocator; AHRE: aryl hydrocarbon response element; CYP1A1: cytochrome P450 1A1; CYP1B1: cytochrome P450 1B1; AHRR: aryl hydrocarbon receptor repressor; TIPARP: TCDD-inducible poly ADP-ribose polymerase. Created with BioRender.com.

1.3.1 AHR and Cytochrome P450 1A1 (CYP1A1)

One well known target gene of AHR is CYP1A1, which is commonly used as a biomarker of AHR activation. CYP1A1 is part of the phase I enzymes Cytochrome P450 superfamily and functions by introducing a hydroxyl group (-OH) to organic compounds (36). This process allows for further metabolism by phase II conjugation enzymes increasing water solubility and ultimately the excretion of the compounds. However, if the detoxifying enzymes are overwhelmed, an accumulation of toxic metabolites could occur. For example, benzo[*a*]pyrene (B[*a*]P) (Figure 3) is a procarcinogenic chemical found in diesel exhaust, cigarette smoke and charbroiled food, which is metabolized to a carcinogenic B[*a*]P-7,8-diol,10-epoxide, leading to DNA-adduct formation and mutation (25, 36).

1.4 AHR ligands

AHR ligands can be divided into exogenous and endogenous, and into agonists and antagonists. TCDD and other planar halogenated polycyclic hydrocarbons and polycyclic aromatic hydrocarbons are examples of exogenous agonists. In addition to xenobiotics, a number of other compounds bind and activate or in some cases inhibit AHR, including dietary ligands, ligands produced by the microflora and endogenous ligands, like the tryptophan metabolite kynurenine (KYN).

1.4.1 Dietary AHR ligands

Humans are exposed to AHR ligands through the diet every day, and their effect on the AHR pathways are diverse and an interesting topic of research. Dietary AHR ligands consist predominantly of phytochemicals, like indoles, flavonoids and carotenoids (19). Cruciferous vegetables like broccoli, cabbage and kale among others, contain considerable amounts of bioactive compounds. Among these is the weak AHR agonist indole-3-carbinol (I3C) that emerges from enzymatic breakdown of glucobrassicin during plant storage and preparation. In the stomach I3C undergoes acid-catalyzed condensation into oligomers, such as 3,3'-diindolylmethane (DIM), 5,11-dihydroindolo-[3,2-*b*]carbazole (ICZ) and a cyclic triindole (37). DIM and ICZ are AHR agonists, however, they have different affinities for the receptor. ICZ has almost as high affinity for AHR as TCDD, while the affinity of DIM is weak (37, 38). DIM, however, comprises 60% of the I3C metabolites (Figure 3) (39). DIM has been shown to mediate its effect through AHR primarily through inhibition of ERα expression and signaling, rather than sustained induction of CYP1A1 expression as other xenobiotic AHR ligands (40). DIM thereby inhibits proliferation of ER^+ breast cancer cells. DIM has several other effects

than being an AHR agonist, as opposed to TCDD. DIM is an anti-oxidant and reduced inflammatory bowel disease in a breast cancer gene 1 (BRCA1) dependent manner (41, 42). In addition, a formulated DIM with higher bioavailability inhibited mammalian target of rapamycin and protein kinase B activity, and nuclear translocation of β-catenin in prostate cancer cells, and thereby decreased cell proliferation (43, 44).

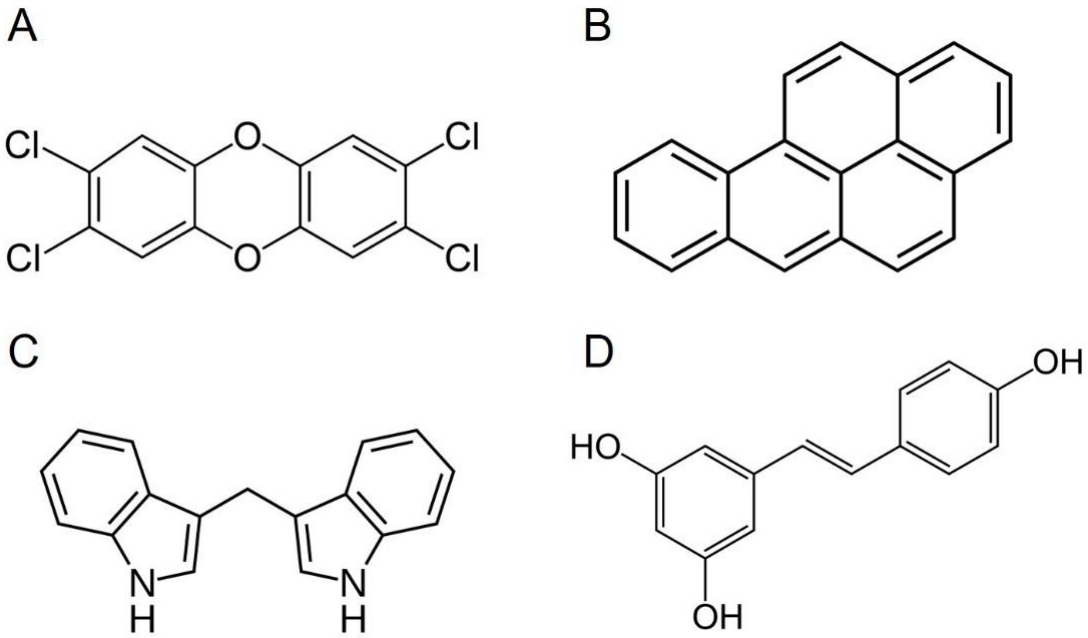

Figure 3. Structure of AHR ligands. A 2,3,7,8-tetrachlorodibenzo-*para*-dioxin (TCDD). **B** Benzo[*a*]pyrene (B[*a*]P). **C** 3,3'-diindolylmethane (DIM). **D** Resveratrol (RES).

Another dietary group of bioactive compounds is the polyphenols. A rather interesting compound is the non-flavonoid polyphenol resveratrol (RES, 3,4',5-trihydroxy-*trans*-stilbene), which has been investigated for its anti-oxidant, anti-inflammatory, cardioprotective and anti-cancer properties (45). The main food sources of RES are in the skin of red grapes and red wine. Consequently, RES has been investigated as a part of the "French paradox" (45). This theory was developed in 1992 as epidemiological data showed a decreased incident of coronary heart disease in the French population, despite saturated fat intake, serum cholesterol, blood pressure and prevalence of smoking at the same level as other countries. The low incident of coronary heart disease was suggested as a consequence of moderate intake of red wine, due to its levels of polyphenols (46). RES acts as an antagonist of AHR, thereby inhibiting expression of target genes like *CYP1A1* (45). However, the bioavailability of RES is low *in vivo* due to rapid metabolism. Nonetheless, subcutaneous injection of equal amounts of the AHR agonists B[*a*]P and 7,12-dimethylbenz[*a*]anthracene and of RES in Sprague-Dawley rats effectively blocked

CYP1A1 expression (47). The rats were injected at day 1 and 7, and sacrifice was done at day 11. Co-treatment with RES completely suppressed CYP1A1 expression in both lung and kidney (47).

Both DIM and RES are also phytoestrogens which activate ER (48). DIM activates both ERα and ERβ, and has been reported to induce ERα-dependent transcription of E2-responsive genes (19). RES is an agonist of both ERα and ERβ, although it has a somewhat higher affinity for ERβ (48). RES mediated activation of ERβ results in elevated levels of quinone reductase, which is a phase II detoxification enzyme that protects against reactive oxygen species (49).

1.5 Role of AHR in breast cancer

AHR is overexpressed and constitutively active in human breast tumors (50). It has also been reported to have a prognostic role for patients with breast cancer that have not metastasized to the lymph nodes, where high levels of AHR correlate with poor overall survival (51). AHR affects cell cycle, immune response, ERα signaling and interacts with BRCA1, a critical tumor suppressor (29).

1.5.1 AHR and ERα

AHR is expressed in both ER^+ and ER^- breast cancer cells (52). AHR inhibits ERα mediated cell proliferation in breast, ovarian and endometrial cancer cells (52). This anti-proliferative effect is widely studied through the AHR-ER cross talk, and the proteins interact in several regards (52, 53). Active AHR recruits ERα to AHRE, away from ERE. In addition, AHR binds to inhibitory AHRE in promotor regions of ER target genes, subsequently inhibiting gene transcription. TCDD treatment induces proteasomal-dependent degradation of ERα, and this effect is further increased with TCDD in combination with E2 (52, 54). Moreover, E2 metabolism and degradation is enhanced by AHR activation, due to increased expression of CYP450 enzymes (55). Co-treatment with E2 and TCDD enhances transcription of AHR target genes compared to TCDD alone. This effect is dependent on ERα and illustrates a feedback regulation of AHR signaling by ERα (53, 56). In addition, some chemicals are dual agonists that activate AHR as well as ERα, including 3-methylcholanthrene and DIM, highlighting another aspect of AHR-ERα cross-talk (53).

1.5.2 AHR and BRCA1

Mutations in the tumor suppressor gene *BRCA1* accounts for approximately 40-45% of hereditary breast cancers and are highly associated with breast and ovarian cancers (57).

Carriers of *BRCA1* gene mutations almost always experience loss of the wildtype (WT) *BRCA1* allele (57). Treatment with the AHR agonist B[*a*]P has been found to inhibit *BRCA1* promotor activity, and reduce BRCA1 protein levels in an AHR- and p23-dependent manner in ER^+ breast cancer (57). In addition, TNBC unlike other breast cancer subtypes, experience CpG hypermethylation of the promotor region of the *BRCA1* gene, which correlates with increased AHR expression. This combination has been suggested as a molecular marker of TNBC (58). Furthermore, BRCA1 directly or indirectly interacts with and stabilizes ARNT to enhance TCDD-dependent transcription of CYP1A1 and CYP1B1 in ER^+ breast cancer (59). BRCA1 and ARNT are recruited to the *CYP1A1* promotor region together with AHR, which is increased with TCDD-treatment. BRCA1 knockdown in ER^+ breast cancer decreases TCDD-induced *CYP1A1* and *CYP1B1* mRNA levels. This suggests that BRCA1 is an important co-regulator of AHR-ARNT dependent transcription in ER^+ breast cancer (59).

1.5.3 Regulation of cell cycle and proliferation by AHR

As mentioned previously, ERα promotes cell proliferation, and AHR's inhibition of ERα consequently has an anti-proliferative role in breast cancer cells. Moreover, AHR closely regulates cell cycle progression and cell proliferation through interaction with cyclin-dependent kinase 4 (CDK4), cyclin D1 (CCND1), retinoblastoma protein (RB1) (60), growth factors (61-63) and β-catenin (64).

In the absence of ligands, AHR is associated with CDK4 and CCND1, and this complex phosphorylates RB1. The hyperphosphorylation of RB1 inhibits its ability to bind and repress E2F transcription factors. Consequently, the cell progresses from the G1 phase into the S phase resulting in increased cell proliferation. However, upon treatment with an AHR ligand, the AHR/CDK4 interaction is disrupted, and the RB1 is hypophosphorylated resulting in G1 cell cycle arrest. This effect has been seen in both ER^+ and ER^- breast cancer (60). In addition, AHR directly interacts with RB1 in an agonist-dependent manner, resulting in decreased phosphorylation (65, 66). Another AHR target gene is *cyclin-dependent kinase inhibitor 1B* which encodes p27, an inhibitor of RB1-phosphorylation (67). *Ahr*-null mouse embryonic fibroblasts (MEFs) are shown to exhibit a delayed progression from G2/M phase of the cell cycle when compared to WT MEFs, spending approximately three times as much time in this phase (68). This delay may be due to AHR's indirect regulation of *cell-division cycle gene 2* (*Cdc2*) and *polo-like kinase* (*Plk*); two proteins that are essential for G2/M phase transition. In addition, *Ahr*-null MEFs have increased transforming growth factor beta levels, which also extends the G2/M phase and decreases proliferation (68).

In addition to regulating the cell cycle, activated AHR also regulates transcription of several growth factors, including vascular endothelial growth factor A, platelet-derived growth factor, epiregulin, amphiregulin and fibroblast growth factor 2 and 9 (61-63, 69).

AHR functions as an agonist-dependent E3 ubiquitin ligase, resulting in proteasomal degradation of β-catenin and disruption of the canonical Wnt-signaling pathway, thereby decreasing proliferation and tumor growth (64). The E3 ubiquitin ligase ability of activated AHR also mediates proteasomal degradation of ERα and androgen receptor in breast and prostate cancer cells, respectively (54). These results were confirmed by *in vivo* studies of mice. Injection of the AHR agonists 3-methylcholanthrene or β-naphthoflavone reduced protein levels of uterine ERα and prostate androgen receptor in mice, despite stable mRNA levels. *Ahr*-null mice experienced no degradation of ER and androgen receptor upon treatment of AHR agonists (54). The sex hormone receptors promote cell proliferation, but they are degraded by an AHR regulated mechanism, ultimately resulting in reduced proliferation.

1.5.4 Migration

A severe complication of breast cancer is metastasis to surrounding organs such as lymph nodes or lungs. A strong contributing factor to metastasis is the epithelial-mesenchymal transition (EMT), which occurs when epithelial cells dedifferentiate and acquire features of mesenchymal cells. EMT plays important roles in embryonic development and in the differentiation of tissues and organs. EMT is also crucial for tissue repair, but it can adversely promote carcinoma progression through many different mechanisms (70). During EMT in cancer, tumor epithelial cells lose their cell-cell adhesion and polarity but gain invasive and migratory properties, making them more like mesenchymal cells. Several mechanisms are necessary for the EMT to occur, including the “cadherin switch” in which expression of the cell-cell anchor molecule E-cadherin is reduced while N-cadherin is increased, the extracellular matrix is degraded by the matrix metalloproteinase (MMP) 1, MMP2, MMP3 and MMP9, the epithelial apical-basal polarity is lost, which together enables migration (71). Transcription factors like SNAI1 (SNAIL), SNAI2 (SLUG), small mothers against decapentaplegic (SMAD) and zinc-finger E-box binding homeobox (ZEB) are critical in mediating EMT (71).

Ligand-dependent activation of AHR has been proposed to contribute to the downregulation of the epithelial cell-cell anchor E-cadherin (72). In addition to being an anchor molecule, E-cadherin sequester β-catenin, and thereby inhibit transcription of genes involved in not only proliferation, but also migration (72). The downregulation of E-cadherin by AHR is mediated

by several pathways. TCDD induces activation of c-Jun NH2-terminal kinase, which has been shown to play a part in methylation of the E-cadherin promotor, and subsequently gene silencing (73, 74). A direct target gene of AHR is SLUG, which downregulates cytokeratine-18, an epithelial marker, and upregulates the mesenchymal marker vimentin. In addition, AHR induces activation of nuclear factor of activated T-cells (NFAT) in a ligand-dependent manner. NFAT promotes transcription of the enzyme autotaxin that generates lysophosphatidic acid, which is known to induce breakdown of E-cadherin junctions (74). Despite these migration promoting properties of activated AHR, there are conflicting results as to whether activation or inhibition of AHR reduces migration and invasion of breast cancer cells *in vitro* and *in vivo* (75-78).

1.5.5 The role of AHR in immune response and tumor microenvironment

The tumor microenvironment is complex, consisting of tumor cells, surrounding blood vessels, fibroblasts, signaling molecules, immune cells and the extracellular matrix. A key enzyme regulating the immune response and vascularization in the tumor microenvironment is indoleamine 2,3-dioxygenase 1 (IDO1) which metabolizes tryptophan into the AHR agonist, KYN. IDO1 is expressed in tumor cells, antigen-presenting cells and stromal cells. Tryptophan depletion and KYN elevation leads to an immunosuppressive environment causing activation of regulatory T cells. The increased levels of KYN induce upregulated transcription of AHR target genes, one of them being *cyclooxygenase II*. Cyclooxygenase II promotes upregulation of IDO1, leading to further KYN accumulation in a positive feedback loop (79, 80). KYN activated AHR also induces the expression of immune check point proteins that suppress the actions of cytotoxic T cells and promote an immunosuppressive tumor microenvironment. Collectively, the actions of AHR allow tumor cells to evade the immune system and allow for increased tumor growth.

Multiple studies support the view that inhibition of AHR would be beneficial in the fight against cancer (81-83). Repressing AHR activation may redirect immunity toward tumor rejection. A number of synthetic and a few natural AHR antagonists are available and are being used to delineate the immunological roles of AHR. In support of this, Bayer Pharmaceuticals recently launched a phase I clinical trial and dose finding study for an AHR antagonist (BAY2416964) in patients with advanced cancer (NCT04069026). The Bayer Pharmaceuticals phase I trial will determine if inhibiting AHR improves immune responses in solid tumors.

1.6 Gene editing technologies

Although pharmacological inhibition is a powerful way to determine the role of AHR in breast cancer, genetic knockout models complement such studies without the potential complication of off-target effects caused by the therapeutic agents. In the past, gene knockout studies were limited to mouse models or other easily manipulated model systems (84). However, the discovery of gene editing approaches allow for the knockout or knockin of virtually any gene in most cell lines and animal models (84). Gene editing technologies have made it possible to specifically manipulate any genomic sequence of interest. There are three main techniques to target and edit a genomic sequence; zinc-finger nucleases (ZFNs), transcription activator-like effector nucleases (TALENs), and clustered regularly interspaced short palindromic repeats (CRISPR)-CRISPR-associated protein (Cas) (Figure 4).

ZFNs were the first widely used gene editing technique (85). They are composed of two custom-designed Cys_2-His_2 zinc-finger proteins, each with a FokI endonuclease. The zinc-finger DNA-binding domain recognize the specific DNA sequence of interest, with each subdomain recognizing a base pair (bp) triplet. FokI cleaves the DNA resulting in a double-stranded break. Two ZFN proteins have to dimerize on opposite DNA strands for FokI to be able to cleave the DNA (85). Much like ZFN, TALENs also require dimerization of TALEN proteins, each composed of a DNA-binding domain and a FokI restriction endonuclease domain that cleaves the DNA strand of interest. TALENs are considered to be more specific and flexible than ZFNs, since each DNA-binding subdomain recognizes one bp instead of three. However due to their large size, they are more challenging to transfect into cells (85).

CRISPR/Cas was initially discovered as an adaptive immune system in bacteria against invading bacteriophages, and later proposed as a new technique for gene editing (86, 87). It was first used in genome editing in 2012 (88), and its popularity has increased exponentially ever since. It is considered the most flexible, effective and specific gene editing technique yet. CRISPR/Cas relies on a specific single-guide RNA (sgRNA) sequence that is complementary to the target gene and thereby directs the associated Cas protein to this site. After the sgRNA binds to the gene sequence of interest, the Cas protein cleaves the DNA, generating a double-stranded break. The only requirement of CRISPR/Cas is that a protospacer adjacent motif (PAM), which is a short DNA sequence, is recognized by Cas proteins that signals them to cleave DNA (85). A PAM motif must be in the targeted genomic sequence and located directly downstream of the 20 nucleotide sgRNA recognition sequence. The PAM sequence is essential for DNA cleavage. There are many different types of Cas proteins which recognizes

specific PAM sequences. One of the most popular is Cas9, which recognizes a 5´-NGG-3´ PAM sequence and is from *Staphylococcus pyogenes*. The reason for CRISPR/Cas' high flexibility and specificity is that the target site recognition is mediated by the sgRNA, and not protein motifs that need to be changed for each target DNA sequence. Unlike ZFNs and TALENs, CRISPR/Cas does not require dimerization to cleave the DNA. Regardless of the method, ZFN, TALENs and CRISPR/Cas9 all generate double-stranded DNA breaks in the target sequence. These are repaired by either non-homologous end joining (NHEJ), generating random insertions or deletions of bp, called indels, or homology-directed repair (HDR) where a new DNA sequence is introduced. By HDR, researchers can introduce a premade DNA sequence and alter the function of the protein, or of the cell, as they wish (85). However, due to the simplicity and low cost, CRISPR/Cas9 generated indels by NHEJ is the preferred method to generate knockout cell lines, and is the method used in this thesis.

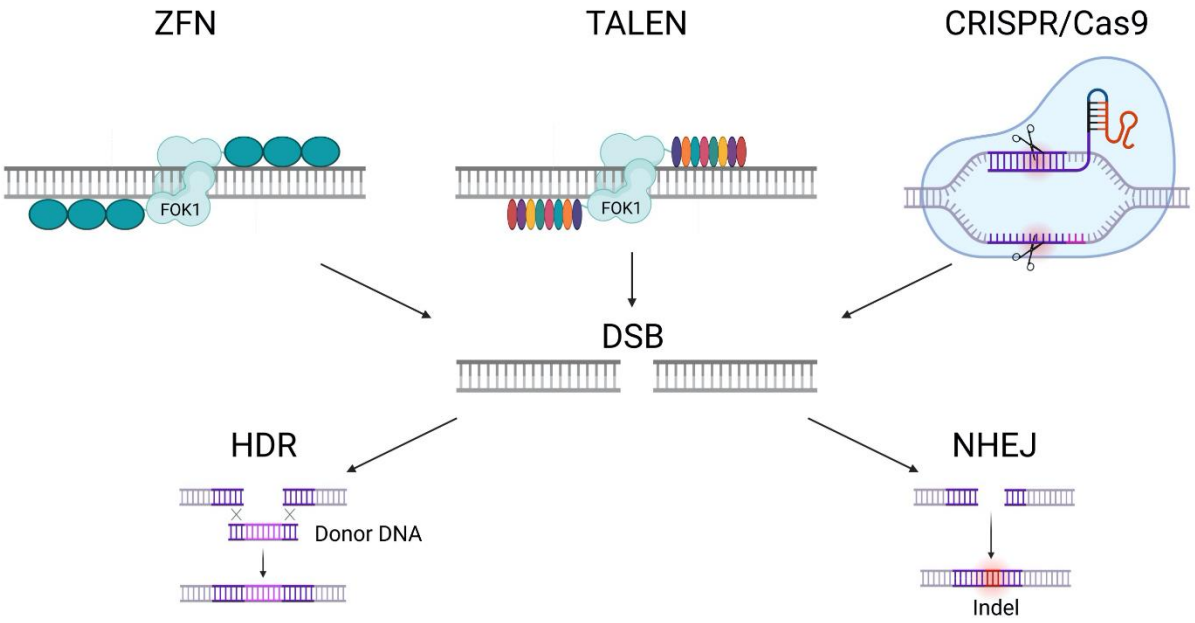

Figure 4. Illustration of different gene editing techniques. Zinc-finger nuclease (ZFN), transcription activator-like effector nuclease (TALEN) and clustered regularly interspaced short palindromic repeats/CRISPR-associated protein 9 (CRISPR/Cas9) all result in double-stranded breaks (DSB). This is repaired by either homology-directed repair (HDR) or non-homologous end joining (NHEJ). HDR can be exploited to introduce DNA into specific genomic locations, while error prone NHEJ leads to the introduction of insertions or deletions (indels). Created with BioRender.com.

2 Project rationale

Breast cancer is a devastating disease in which the prognosis largely depends on the immunohistochemical markers expressed by the breast cancer. TNBCs are the most difficult breast cancer subtype to treat because they lack hormone receptors and HER2, and thus patients have limited therapeutic options. A wide range of studies are therefore investigating alternative treatment options of breast cancer. AHR has been proposed as a potential drug target; however, there are conflicting evidence as to the effect of targeting AHR in breast cancer cells. In addition, several studies focus on the effect of potent AHR agonists, like TCDD and B[*a*]P, although today the exposure to these compounds is marginal. Dietary AHR ligands on the other hand, are consumed on a daily basis in larger amounts than xenobiotics, although the affinity of AHR is decreased. Two promising dietary AHR ligands are DIM, an AHR agonist, and RES, an AHR antagonist. Both ligands are being actively pursued as potential therapeutics against cancer (39, 45). However, they also have many cellular effects that are independent of AHR, and it is not clear whether their anti-cancer effects are mediated through AHR. Therefore, this thesis will further elucidate the effect of AHR on proliferation and migration of ER^+ and ER^- breast cancer cells, using AHR knockout and treatment with the AHR ligands DIM and RES.

3 Hypothesis

The working hypothesis is that pharmacological inhibition or knockout of AHR would be an effective strategy to reduce breast cancer cell proliferation and migration.

This hypothesis was tested in two aims.

3.1 Aims

The overall aim was to examine the effect of AHR loss or its inhibition in ER^+ and ER^- breast cancer cell lines on the proliferative and migratory properties of the cells. This was done using two different strategies:

1. Determine the effect of knockout of AHR on ER^+ and ER^- breast cancer cell lines.
2. Determine the effect of a dietary AHR agonist and antagonist on ER^+ and ER^- breast cancer cell lines.

4 Material and methods

4.1 Chemicals and biological reagents

Dimethyl sulfoxide (DMSO), DIM and RES were purchased from Sigma-Aldrich (St. Louis, MO, USA). TCDD was purchased from AccuStandard (New Heaven, CT, USA). Ribon-2397 (RBN-2397) was purchased from MedChemExpress (Monmouth Junction, NJ, USA) (89). All other chemicals were purchased from Sigma-Aldrich unless stated otherwise. Complete lists of all chemicals, equipment and software programs used are provided in appendix 1.

4.1.1 Cultivation of MCF7, MDA-MB-231 and MDA-MB-468 cell lines

All cell lines used in this study were purchased from the American Type Culture Collection (ATCC, Manassas, VA, USA). The cell lines included were the three human breast cancer cell lines MCF7 (HTB-22), MDA-MB-231 (HTB-26) and MDA-MB-468 (HTB-132). All three cell lines are widely used in *in vitro* breast cancer studies. In addition to the WT cell lines, AHR knockout (AHR^{ko}) cell lines of MCF7 and MDA-MB-231 were made using ZFN technology before I joined the research group (90). We received what we thought were MDA-MB-468 AHR^{ko} cells from Dr. Chiara Gorrini, (Princess Margaret Cancer Centre, 610 University Avenue, Toronto, ON M5G 2M9, Canada), which I will refer to as MDA-MB-468 AHR^{ko} TO. Since the MDA-MB-468 AHR^{ko} TO cells had residual AHR activity, we created new MDA-MB-468 AHR^{ko} cell lines using CRISPR/Cas9.

All cell lines were cultivated in Dulbecco's Modified Eagle's Medium (DMEM) (1.0 g/l glucose) (Lonza, Walkersville, MD, USA) supplemented with 10% (v/v) Fetal Bovine Serum (FBS) (Sigma-Aldrich), 1% (v/v) pencillin-streptomycin (Sigma-Aldrich) and 1% (v/v) L-glutamine (Sigma-Aldrich). All cell lines were maintained in a humidified environment at 37ºC and 5% CO_2, and subcultured when 80% confluence was reached, which was approximately every 2-3 days.

4.1.2 Generation of AHR^{ko} cell lines using gene editing approaches

MCF7 AHR^{ko} cells and MDA-MB-231 AHR^{ko} cells were generated using CompoZr knockout ZFN plasmids targeting exon 1 in the *AHR* gene (CKOZFND26436; Sigma-Aldrich) as previously described (90). The MDA-MB-468 AHR^{ko} cell line was generated using CRISPR/Cas9. Briefly, the following guide oligos were designed to express the sgRNA; forward primer 5´-CCTACGCCAGTCGCAAGCGG-3´ and reverse primer 5´-CCGCTTGCGACTGGCGTAGG-3´ targeting exon 1 of *AHR*. The sgRNA binding site was

in close proximity to the ZFN recognition sites used to generate the MCF7 AHR^{ko} and MDA-MB-231 AHR^{ko} cells. The sgRNA was cloned into the pSpCas9(BB)-2A-Puro (PX459) plasmid (Addgene, Watertown, MA, USA; plasmid #62988), containing *Streptococcus pyrogenes* (Sp) Cas9 and puromycin genes. The PX459 AHR containing gRNA plasmid was transfected into MDA-MB-468 cells, using Lipofectamine 2000 (Invitrogen, Carlsbad, CA, USA). Three days after transfection, the cells were exposed to 1 µg/mL puromycin for 4 days at 37°C and 5% CO_2. The puromycin containing medium was exchanged with normal DMEM with 10% FBS medium and the cells were allowed to expand for 5 days. Some of the cells were used to confirm the efficiency of the gRNA at targeting *AHR* with a T7 endonuclease assay. The cells were diluted to 10 cells/well in a 1 x 96-well plate and colonies were expanded. TCDD dependent increase in *CYP1A1* mRNA were used to screen for AHR^{ko} clones by reverse transcription-quantitative Polymerase Chain Reaction (RT-qPCR) as described below.

4.1.3 T7 endonuclease assay

To perform this experiment, GenElute™ Mammalian Genomic DNA Miniprep Kits (Sigma-Aldrich) was used to isolate genomic DNA (gDNA) from different breast cancer cell lines according to manufacturer's instructions. The AHR gene was amplified by PCR GC-RICH PCR System kit (Sigma-Aldrich) according to manufacturer's instructions. The following reaction conditions were set at a thermal cycler: 95°C for 3 minutes, 95°C for 30 seconds, 55°C for 30 seconds, 72°C for 45 seconds, 72°C for 7 minutes. Step 2-4 were repeated 35 times. AHR primers used were the following: forward 5´-CACTGTCCCGAGAGGACG-3´ and reverse 5´-GGGAATGGACCTAATCCCAG-3´. The PCR-product was analyzed by agarose gel electrophoresis using a 1% agarose gel and 80 V for 18 minutes. The band containing the AHR^{ko} gene was cut out and a PCR gel clean-up was performed using NucleoSpin® Gel and PCR Clean-up kit (Macherey-Nagel, Düren, Germany) according to manufacturer's instructions. The T7 endonuclease I (New England Biolabs, Ipswich, MA, USA) was then used to detect mutations in the PCR-product as a result of premature stop codons in the MDA-MB-231 AHR^{ko} and MDA-MB-468 AHR^{ko} cell lines. Twelve µl of the PCR-product was combined with 2 µl NEBuffer™ 2 (New England Biolabs) and 4 µl of H_2O (Sigma-Aldrich). This was set on a thermal cycler with the following reaction settings: 95°C for 10 minutes, 85°C for 5 seconds, and then a decrease of the temperature of 2°C/second prior to 25°C for 5 seconds, and then a new decrease of 0.1°C/second until a hold on 4°C. Two µl of the T7 Endonuclease I enzyme were added, followed by incubation of the mixture at 37°C for 40 minutes. Four µl of 6x loading

dye was added, and 10 µl was then separated on a 7% polyacrylamide gel using 75 V for 60 minutes.

4.1.4 Sequencing of mutations in the *AHR* gene in AHR^{ko} cell lines

To confirm frameshift mutations in the gene edited cell lines, the exon 1 of the *AHR* gene in MDA-MB-231 AHR^{ko} and MDA-MB-468 AHR^{ko} cells were sequenced. Isolation of gDNA, PCR amplification and PCR gel clean-up was performed as previously described (90). The PCR-product was ligated into PCR vector pCR2.1 (Invitrogen). The reaction was incubated at 4°C over-night. The next day the vector was transformed into 5-alpha competent *E.coli* bacteria (New England Biolabs). The bacteria were grown on agar plates containing 50 µg/ml kanamycin (Sigma-Aldrich). Bacteria colonies were picked from the agar plate and grown in lysogeny broth medium supplemented with 50 µg/ml kanamycin. Miniprep was then performed using NucleoSpin Plasmid Mini kit (Macherey-Nagel) according to manufacturer's instructions. The isolated plasmids were diluted to a concentration of 150 µg/µl and mixed with 5 µl M13 reverse primer (ThermoFischer Scientific, Waltham, MA, USA) in a 1:1 ratio. The M13 reverse primer sequence was 5´-CAGGAAACAGCTATGAC-3´. Sanger sequencing of the gene sequence was done by Eurofins Genomics with LightRun Tube.

4.1.5 RNA isolation, cDNA and RT-qPCR

The cells were seeded in a 12-well plate at a density of 1.25×10^5 cells per well and incubated 24 hours at 37°C and 5% CO_2. AHR ligands were added to the wells and incubated 24 hours prior to harvesting. High-quality DNA-free total RNA were isolated using the Aurum™ Total RNA isolation kit (BioRad, Hercules, CA, USA) according to manufacturer's instruction. The RNA was reverse transcribed into single-stranded complementary DNA (cDNA) using the High-Capacity cDNA Reverse Transcription Kit (Applied Biosystems, Foster City, CA, USA) according to manufacturer's instruction. A thermal cycler was used to make the cDNA with the following settings: 25°C for 10 minutes, 37°C for 120 minutes, 85°C for 5 minutes and 4°C on hold. RT-qPCR was performed using 5 µl Sso Advanced™ Universal SYBR® Green Supermix (BioRad), 0.1 µl of both the forward and reverse gene specific primers (Sigma-Aldrich), 1 µl of diluted cDNA, and H_2O (Sigma-Aldrich) to a final volume of 10 µl per reaction. Reactions were set on a 96-well PCR plate in two technical replicates. A thermal cycler was used with the following settings: 95°C for 5 minutes, 95°C for 10 seconds and 60°C for 20 seconds, where the last two steps were repeated in 45 cycles. Primers used to amplify genes were; *CYP1A1* forward 5´-TGGTCTCCCTTCTCTACACTCTTGT-3´ and reverse 5´-ATTTTCCCTATTACATTAAATCAATGGTTCT-3´, *CDH1* forward 5´-

GAACAGCACGTACACAGCCCT-3´ and reverse 5´-GCAGAACTGTCCCTGTCCCAG-3´, *CDH2* forward 5´-GGCATAGTCTATGGAGAAGT-3´, and reverse 5´-GCTGTTGTCAGAAGTCTCTC-3´, and *Tata-binding protein* forward 5´-TTGTACCGCAGCTGCAAAAT-3´ and reverse 5´- TATATTCGGCGTTTCGGGCA-3´. All target transcripts were normalized to the housekeeping gene *Tata-binding protein* and analyzed using the comparative CT method (ΔΔCT).

4.1.6 Western blot

Cells were seeded in a 6-well plate at a density of 2.5×10^5 cells per well and incubated 48 hours at 37°C and 5% CO_2. Three wells were pooled together while harvesting cells to make one cell pellet. The cell pellet was dissolved in 200 µl of 1x radioimmunoprecipitation assay buffer (Cell Signaling Technology, Danverse, MA, USA) supplemented with 2x protease inhibitor cocktail (Roche Diagnostics, Mannheim, Germany) and 2 mM dithiothreitol (ThermoFischer Scientific). The samples were sonicated at low intensity for 2 x 30 seconds on/off, prior to rotation for 10 minutes and centrifuging for another 10 minutes. 4x Laemmli Sample Buffer (BioRad) supplemented with 2-Merchaptoethanol (Sigma-Aldrich) was added in a 1:3 ratio, prior to heating at 95°C for 5 minutes. The lysed cells were frozen at -20°C until further use. Protein concentrations of the samples were determined prior to adding Laemmli Sample buffer by using the Pierce™ bicinchoninic acid Protein Assay Kit (ThermoFischer Scientific), with Pierce™ Bovine Serum Albumin (ThermoFischer Scientific) as protein standards.

The samples were loaded with a protein concentration of 20 µg into a Criterion™ TGX™ Precast SDS-PAGE gel (BioRad) with an acrylamide concentration of 10%, and separated using 150 V for 90 minutes. The proteins were transferred to an Immobilon-P polyvinylidene fluoride membrane (MerckMillipore, Burlington, MA, USA) by wet electroblotting at 600 mA for 60 minutes. The membrane was blocked with 5% skimmed milk (Sigma-Aldrich) for 60 minutes at room temperature. After blocking, the membrane was incubated with a primary antibody against the protein of interest overnight at 4°C. The following primary antibodies were used: α-AHR (rabbit, Enzo Life Sciences, Farmingdale, NY, USA, cat: bml-sa210-0100, lot: 04011942) in the ratio of 1:8000, and anti-β-actin (mouse, Sigma-Aldrich, AC-74, cat: A2228-200UL lot: 099M4776V) in the ratio of 1:5000. The membrane was washed 4 x 10 minutes with the washing buffer TBS-T, prior to incubation with the respective horseradish peroxidase labelled secondary antibody (Cell Signaling Technology) at a 1:2000 ratio for 60 minutes at room temperature. The membranes were then washed 4 x 10 minutes with TBS-T. The proteins were visualized with SuperSignal™ West Pico PLUS Chemiluminescent

Substrate (ThermoFisher Scientific), SuperSignal™ West Dura Extended Duration Substrate (Thermo Fisher Scientific) or SuperSignal™ West Femto Maximum Sensitivity Substrate (ThermoFisher Scientific) by using enhanced chemiluminescence detection.

4.1.7 7-ethoxyresorufin-O-deethylase (EROD) cell bioassay

The 7-ethoxyresorufin-O-deethylase (EROD) (Sigma-Aldrich) cell bioassay was used to determine the activity of the CYP1A1 enzyme in the cells. Cells were plated in a 96-well plate with a density of 1×10^4 cells/well using a multichannel pipette. The cells incubated 24 hours at 37°C and 5% CO_2. The next day the medium was replaced with new medium containing DMSO or AHR ligands and incubated for 24 hours. On the following day, a 7-ethoxyresorufin (ETX) working solution consisting of 200 µl of 400 µM ETX (Sigma-Aldrich), 50 µl of 2 mM dicoumarol and 10 ml room tempered Tris buffer (50 µM, pH 8.0) was prepared for each plate. The cell culture medium was removed and 100 µl of ETX working solution was added. The plate incubated 45 minutes at 37°C in the dark. To stop the reaction, 75 µl of cold methanol was added and incubated for 2 minutes in the dark under gentle shaking. Conversion of ETX to resorufin was determined by fluorescence spectrophotometry with excitation wavelength at 540 nm, and emission wavelength at 590 nm. Pierce™ Bovine Serum Albumin (ThermoFischer Scientific) was used to make a protein concentration standard curve. The protein concentration was determined by adding 100 µl of Pierce™ bicinchoninic acid Protein Assay Kit (ThermoFischer Scientific) to each well. Absorbance was measured at 562 nm after 45 minutes incubation. The EROD activity was calculated by the following equation, where *FU* is fluorescence intensity, *t* is incubation time and *C Protein* is the protein concentration.

$$EROD = FU/t \times C\ Protein$$

4.1.8 Proliferation assay

The cells were plated in 2 x 96-well plates with opaque walls and clear bottom, at a density of 4000 cells/well in 100 µl DMEM/well. Proliferation was measured at baseline and after 72 hours. Accordingly, the cells were plated in two different plates, one for each time measurement. Approximately 5-6 hours after plating, when the cells had attached, the baseline measurement was recorded. In addition, the medium was replaced in the second 96-well plate, and DMSO or AHR ligands were added. The medium was carefully aspirated and replaced with new medium containing ligands every 24 hours. The CellTiter-Glo® Luminescent Cell Viability Assay (Promega, Madison, WI, USA) was used to measure grade of proliferation according to manufacturer's instructions. The data was normalized to the baseline measurements.

4.1.9 Migration assay (Scratch assay)

The cells were plated in a 12-well plate at a density of 3×10^5 cells/well. After 24 hours, a scratch was made in each well by moving a 1000 µl pipette tip vertically from the top of the well to the bottom at a 90° angle. The medium was then aspirated and replaced with new medium supplemented with 1% FBS to limit cell proliferation and containing DMSO or AHR ligands. The medium and ligands were changed every 24 hours. Images of the scratches were taken at baseline when the scratch was made, and after 72 hours. Each ligand treatment and the DMSO control was replicated three times, and three images were taken per well to control for in-well variability. The area of the scratch was measured using ImageJ version 1.53e (Wayne Rasband and contributors, National Institutes of Health, USA) with the Wound Healing Size Tool plugin expansion developed by Suarez-Arnedo et al. (91).

4.2 Statistics

All statistics were carried out using GraphPad Prism version 8.3.0 (San Diego, CA, USA). Significant differences were identified by Student's t-test, one-way analysis of variance (ANOVA) or two-way ANOVA, followed by either Tukey's or Sidak's multiple comparisons test. Appropriate non-parametric tests were used when the data did not pass Shapiro-Wilk test for normality. Significant differences were set to $p<0.05$. All data is provided as mean ± standard deviation of the mean (SEM) of three independent replicates.

5 Results

5.1 Confirmation of AHR^{ko} cell lines

To ensure that the MCF7, MDA-MB-231 and MDA-MB-468 gene edited clones were devoid of AHR, I first confirmed that AHR was knocked out in the different cell lines. The lab group has three criteria that the cell lines had to pass to be eligible for further studies: (1) no TCDD inducible *CYP1A1* mRNA expression; (2) no detectable AHR protein expression; and (3) confirmed frameshift mutations and the presence of a premature stop codon determined by DNA sequencing. Since the MCF7 AHR^{ko} cells are routinely used by the lab group, and the lack of AHR expression was recently confirmed, I did not need to reconfirm them for my thesis. The MDA-MB-231 AHR^{ko} cells, however, have not been actively used in several years. We originally received MDA-MB-468 AHR^{ko} cells from collaborators in Toronto, Canada, that I refer to as MDA-MB-468 AHR^{ko} TO. Unfortunately, these cells failed to meet our three criteria (Figure 5). TCDD treatment caused a weak, but significant increase in *CYP1A1* mRNA levels indicating that the cell line had residual or very low AHR activity (Figure 5). AHR protein was detected by western blotting in extracts from MDA-MB-468 WT cells, but similar experiments from MDA-MB-468 AHR^{ko} TO cells were inconclusive. There appeared to be a weak AHR band, but it was difficult to be certain due to the low signal, despite using the most sensitive western developing solutions I had available in the lab (Figure 5). I next sequenced DNA of the 345 bp AHR indel amplicon that included both the ZFN and sgRNA recognition sequences in exon 1 of *AHR*. However, DNA sequencing of the MDA-MB-468 AHR^{ko} TO cells revealed that at least 1/20 sequences had a loss of 12 bp, resulting in a loss of four amino acids at positions 10 to 13 in the AHR, with no shift in the reading frame (Figure 5). Therefore, I used CRISPR/Cas9 to generate a new MDA-MB-468 AHR^{ko} cell line.

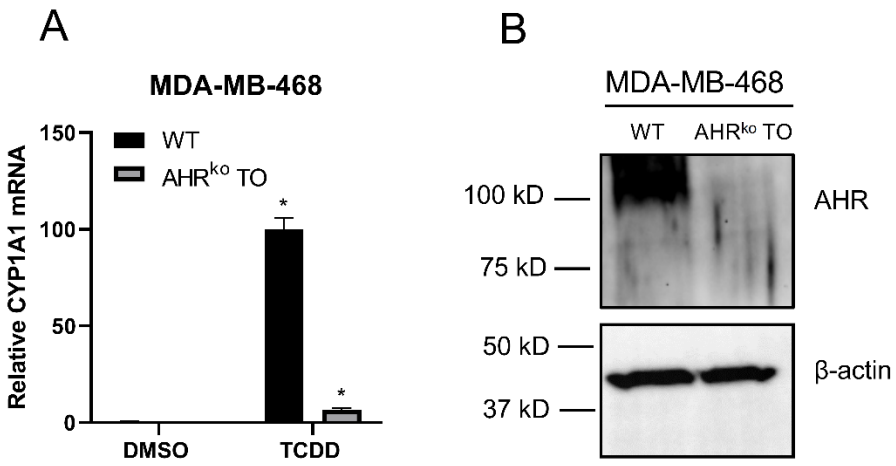

C

MDA-MB-468 AHR^{ko} TO

```
Exon1                                                    Exon2
aacatcacctacgccagtcgcaagcggcggaagccggtgcagaaaacagtaaagccaatcccagctgaaggg      wildtype
 N7 I  T  Y  A  S  R  K  R  R  K  P  V  Q  K  T  V  K  P  I  P  A  E
aacatcac----------caagcggcggaagccggtgcagaaaacagtaaagccaatcccagctgaaggg   12 deletion
 N7 I  T              K  R  R  K  P  V  Q  K  T  V  K  P  I  P  A  E
aacatcacctacgcc-------agcggcggaagccggtgcagaaaacagtaa                     7 deletion
 N7 I  T  Y  A         S  G  G  S  R  C  R  K  Q  Stop
aacatcacctacgccagtcgcaaaagcggcggaagccggtgcagaaaacagtaa                   2 insertion
 N7 I  T  Y  A  S  R  K  S  G  G  S  R  C  R  K  Q  Stop
aacatcacctacgccagtcgccaagcggcggaagccggtgcagaaaacagtaaagccaatcccagctga    1 insertion
 N7 I  T  Y  A  S  R  Q  A  A  E  A  G  A  E  N  S  K  A  N  P  S  Stop
aacatcacctacgccagtcggcaagcggcggaagccggtgcagaaaacagtaaagccaatcccagctga    1 insertion
 N7 I  T  Y  A  S  R  Q  A  A  E  A  G  A  E  N  S  K  A  N  P  S  Stop
```

Figure 5. Screening of MDA-MB-468 AHR^{ko} TO cells revealed weak AHR activity. A *CYP1A1* mRNA levels generated by RT-qPCR. MDA-MB-468 WT and MDA-MB-468 AHR^{ko} TO cells were treated with DMSO or 1 nM TCDD. Fold change was calculated using the ΔΔCT method and are presented as mean ± SEM of n=6 replicates normalized to 100% of MDA-MB-468 WT cells treated with TCDD. Significant differences were detected by two-way analysis of variance (ANOVA). * illustrates significant differences compared to WT DMSO ($p<0.05$). **B** Protein levels of AHR generated by western blotting. β-actin was used as loading control. **C** DNA sequencing of the *AHR* indel amplicon presented from the seventh amino acid. A deletion of 12 bp was revealed, resulting in no frame shift mutation and no premature stop codon. Exon 1 is written in black, exon 2 in blue. Indels are marked with red lettering, dashes illustrate deletion and letters illustrate insertion. Amino acids affected by the indels are marked in italic. Premature stop codons are marked with "*Stop*".

Before confirming the knockout of AHR in the MDA-MB-231 gene edited cells and the newly gene edited MDA-MB-468 cells, I performed a T7 endonuclease mismatch assay on the

PCR-product of MDA-MB-231 AHR^{ko} and MDA-MB-468 AHR^{ko} cells to detect potential insertions or deletions in the *AHR* gene. For MDA-MB-231 WT and MDA-MB-468 WT cells, a single band at 345 bp was detected in extracts from the cells by 7% PAGE. In addition to the 345 bp band, two smaller bands were also observed in extracts from MDA-MB-231 AHR^{ko} and MDA-MB-468 AHR^{ko} cells (Figure 6). These smaller bands were the result of cleavage of the DNA at mutated sites by T7 endonuclease enzyme, which detects bulges in DNA sequences resulting from non-complementary sequences in which one contains indels or mutations. Similar findings have been observed and reported of the MCF7 AHR^{ko} cell line (90).

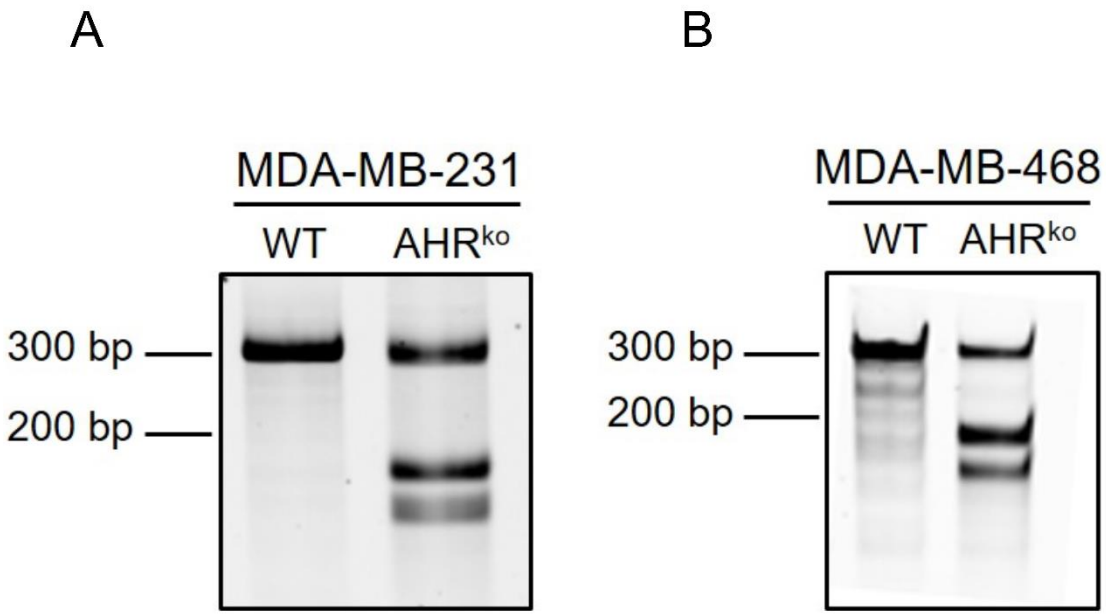

Figure 6 T7 endonuclease digestion of MDA-MB-231 and MDA-MB-468 cells. A MDA-MB-231 WT and MDA-MB-231 AHR^{ko} generated by ZFN technology. **B** MDA-MB-468 WT and MDA-MB-468 AHR^{ko} generated by CRISPR/Cas9 after puromycin selection, but before dilution cloning. The T7 endonuclease system detected bulges in the DNA of the two AHR^{ko} cell lines, resulting in endonuclease activity and subsequently smaller DNA fragments. Such bulges were not detected in the WT cell lines, resulting in only one band.

Next, I checked the three criteria for confirming the knockout of AHR in the cell lines. I first determined the AHR-dependent induction of *CYP1A1* mRNA levels by treating the different WT or AHR^{ko} cell lines with 1 nM of TCDD for 24 hours. This confirmed that there was no TCDD-induced increase in *CYP1A1* mRNA levels in the MCF7 AHR^{ko} and MDA-MB-231 AHR^{ko} cells (Figure 7A and 7B). As expected, *CYP1A1* gene expression was increased in MCF7 WT and MDA-MB-231 WT cells when treated with TCDD compared with DMSO. In addition, I treated the cells with a combination of 1 nM TCDD and 0.1 µM of an inhibitor of

TIPARP, RBN-2397, for 24 hours. AHR is negatively regulated by TIPARP. RBN-2397 is a potent TIPARP inhibitor (89), and by inhibiting TIPARP we ultimately increase the activity of AHR. If the AHR^{ko} cell lines had any residual AHR activity that was downregulated by TIPARP, it would be noticeable upon TIPARP-inhibition in combination with a potent AHR agonist like TCDD. The combination of TCDD and RBN-2397 would result in an even larger increase in the fold change of *CYP1A1* mRNA than treatment with TCDD alone. This was observed with MCF7 WT and MDA-MB-231 WT cells (Figure 7A and 7B). As expected, no such increase was observed in MCF7 AHR^{ko} or MDA-MB-231 AHR^{ko} cells, which further arguments the knockout of the AHR protein in these cell lines. To screen the dilution clones of the CRISPR/Cas9 generated MDA-MB-468 AHR^{ko} cells, we co-treated the cells directly with 1 nM TCDD and 0.1 µM RBN-2397. Among the different dilution clones of MDA-MB-468 AHR^{ko}, two did not express any AHR activity (Figure 7C). These were located in well B1 and C3 on the 96-well plate and named thereafter.

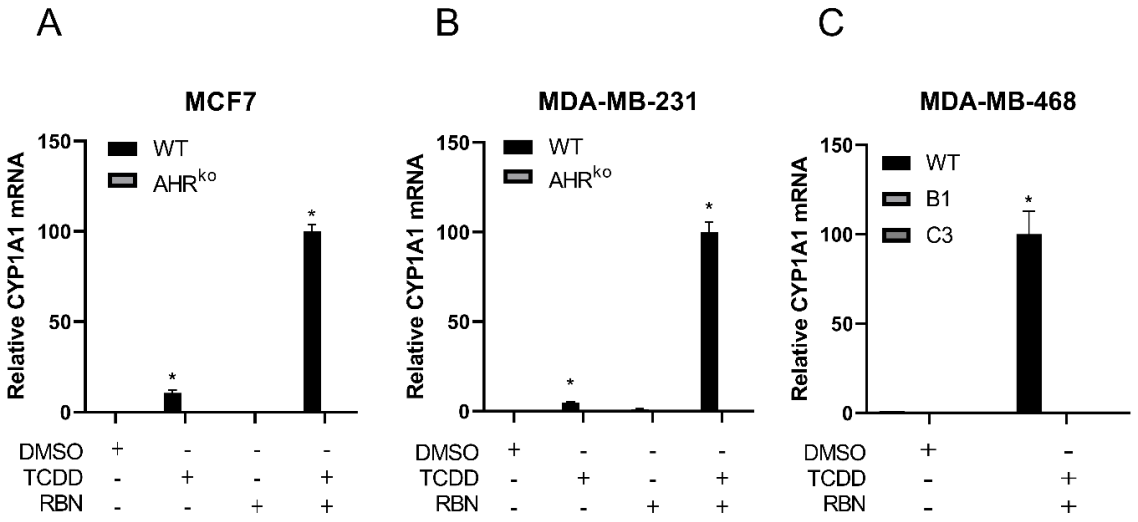

Figure 7. Gene expression of *CYP1A1* mRNA generated by RT-qPCR of WT and AHR^{ko} cell lines of (**A**) MCF7, (**B**) MDA-MB-231 and (**C**) MDA-MB-468 with the two AHR^{ko} dilution clones B1 and C3. MCF7 and MDA-MB-231 cells were treated with DMSO as control, 1 nM of TCDD, 0.1 µM of RBN-2397 (RBN) or a combination of TCDD and RBN-2397. MDA-MB-468 WT cells and the MDA-MB-468 AHR^{ko} dilution clones B1 and C3 were treated with DMSO or the combination of TCDD and RBN-2397. Fold change was calculated using the ΔΔCT method and are presented as mean ± SEM of n=6 replicates (**A** and **B**), and n=2 replicates (**C**). The y-axis is fold change normalized to 100% of the corresponding WT co-treated with TCDD and RBN-2397. Significant differences were detected by two-way analysis of variance (ANOVA). * illustrates significant differences compared to WT DMSO ($p<0.05$).

In agreement with RT-qPCR, western blots of MCF7 AHR^{ko} and MDA-MB-231 AHR^{ko} cells did not display any AHR protein (Figure 8). MDA-MB-468 AHR^{ko} cells were generated in the second half of the research year. Western blotting to confirm the loss of AHR protein levels has not been completed yet.

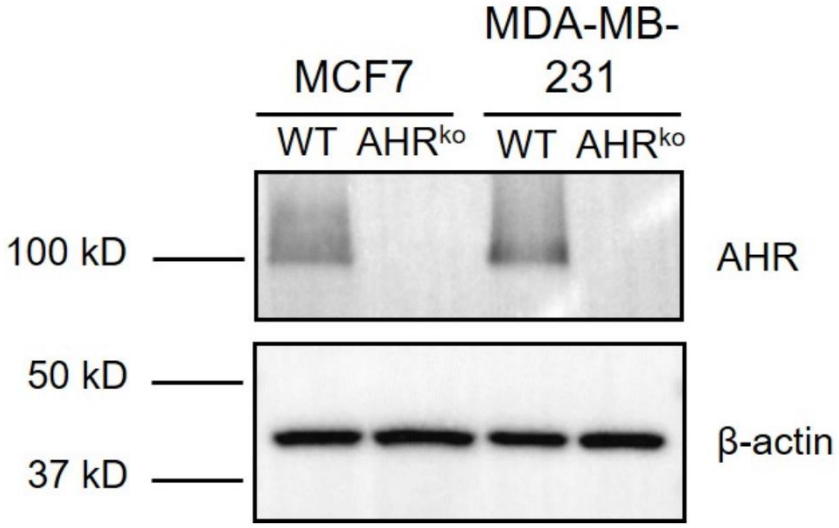

Figure 8. Protein levels of AHR in MCF7 WT and MCF7 AHR^{ko} cells, and MDA-MB-231 WT and MDA-MB-231 AHR^{ko} cells. AHR has a protein mass of ~96 kDa and is not detectable in the lanes containing AHR^{ko} cells. β-actin was used as loading control.

Lastly, I used DNA sequencing to ensure that the *AHR* indel amplicons from the different AHR^{ko} cell lines contained frame shift mutations in the *AHR* gene, resulting in no AHR protein expression. DNA sequencing of the *AHR* indel amplicon from MDA-MB-231 AHR^{ko} cell lines identified three different indels that resulted in frameshift mutations; a 11 bp deletion, a 2 bp deletion, and a 2 bp insertion (Figure 9B). The 11 bp and 2 bp deletions were previously reported in the original characterization of the cell lines (90). However, the 2 bp insertion was newly identified in this thesis. These indels were different from 20 bp and 4 bp loss observed in the MCF7 AHR^{ko} cell line (90), which have been included for comparison (Figure 9A). The DNA of the *AHR* indel amplicon of the two MDA-MB-468 AHR^{ko} dilution clones, B1 and C3, were sequenced, and resulted in the following mutations; a 1 bp deletion, a 10 bp deletion, a 14 bp deletion, and a 20 bp deletion (Figure 9C). All mutations resulted in a premature stop codon (Figure 9). Since all three criteria are fulfilled, we can conclude that MCF7 AHR^{ko} and MDA-MB-231 AHR^{ko} cells have no functional AHR protein and are eligible for further analyses. The newly generated MDA-MB-468 AHR^{ko} cell line has not yet been checked for protein level by western blotting due to time limitations. Consequently, they were not included

in any further analyses examining the effect of dietary ligands, or of proliferative and migratory properties.

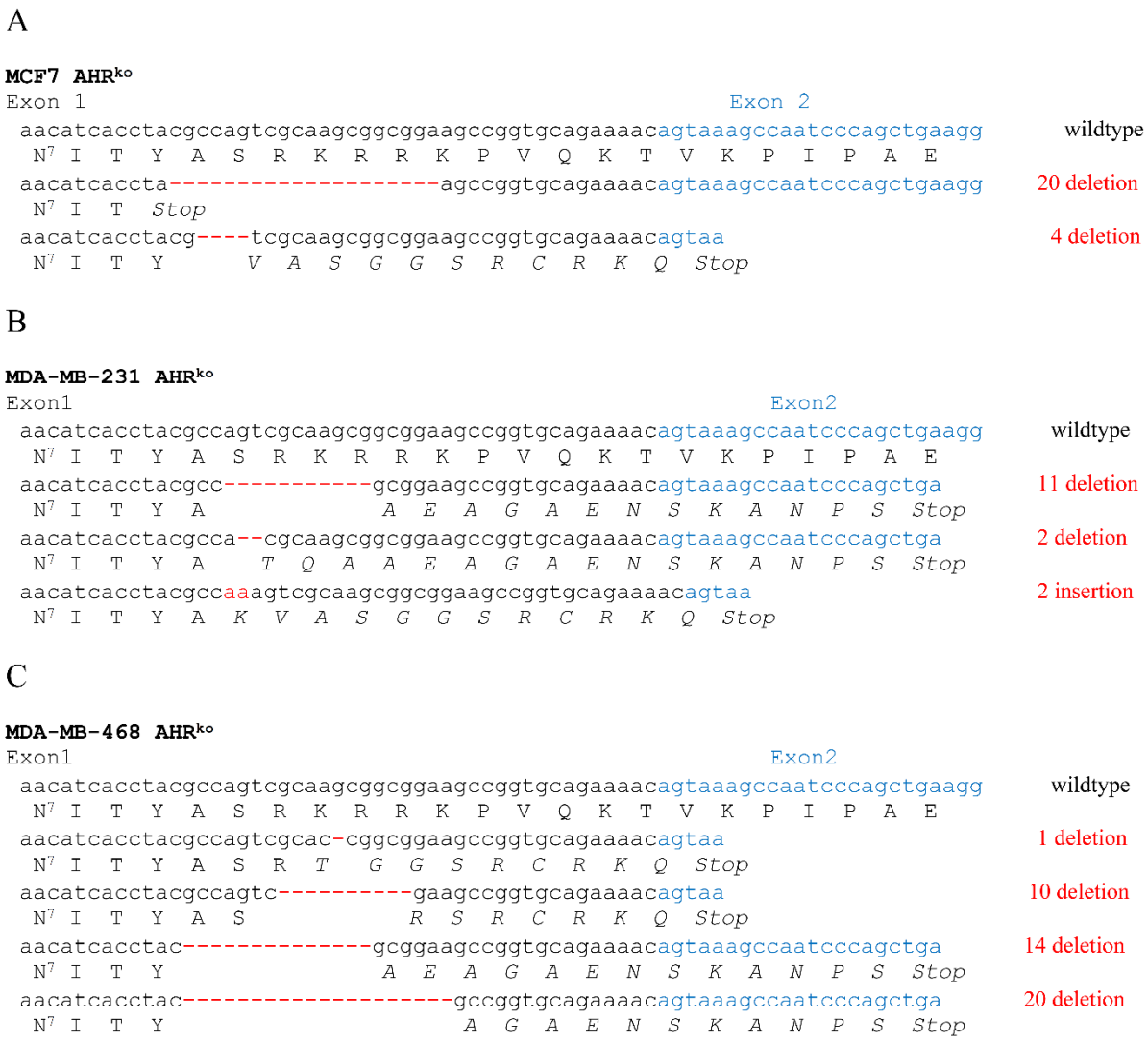

Figure 9. Sequencing data of *AHR* indel amplicon of (**A**) MCF7 AHR^{ko} cells, (**B**) MDA-MB-231 AHR^{ko} cells and (**C**) MDA-MB-468 AHR^{ko} clone B1 and C3 presented from the seventh amino acid. MDA-MB-468 AHR^{ko} clone B1 and C3 had the exact same mutations. Exon 1 is written in black, exon 2 in blue. Indels are marked with red lettering, dashes illustrate deletion and letters illustrate insertion. Amino acids affected by the indels are marked in italic. Premature stop codons are marked with "*Stop*".

5.2 Combination treatment of DIM and RES increase transcription, but not activity, of CYP1A1

To examine the effect of the dietary AHR ligands DIM and RES on the canonical AHR pathway, I performed RT-qPCR to determine the mRNA level of *CYP1A1*. As described above, no *CYP1A1* mRNA levels were observed in MCF7 AHR^{ko} cells or MDA-MB-231 AHR^{ko} cells upon treatment with TCDD, which was also true for the dietary AHR ligands. Therefore, only results from the MCF7 WT and MDA-MB-231 WT cell lines are presented (Figure 10A and 10B). The data are presented as normalized to 100% of the TCDD WT values for each cell line, however, TCDD increased CYP1A1 transcription more in MCF7 WT cells with an average fold change of 5812 relative to the DMSO control, compared to an average fold change of 47 for MDA-MB-231 WT cells (n=6). The dietary AHR ligands have a lower affinity for AHR than TCDD (92). The dose of 10 μM DIM was chosen based on previous studies showing that this concentration caused maximum induction of *CYP1A1* mRNA levels without any cell toxicity, in addition to being the physiological relevant blood concentration (93, 94). Similarly, the dose of 10 μM RES was chosen since it was previously reported by our lab group to effectively antagonize 1 nM TCDD-dependent induction of *CYP1A1* mRNA levels (95). The doses of TCDD, which was used as positive control for AHR activation, were 1 and 10 nM with the latter resulting in maximum activation of AHR.

As expected, 24 hours treatment with 1 nM TCDD significantly increased *CYP1A1* mRNA levels in MCF7 WT cells (Figure 10A). Treatment with 10 μM DIM alone also significantly increased *CYP1A1* mRNA levels in MCF7 WT cells, but to only approximately 10% that of TCDD (Figure 10A). Treatment with 10 μM RES did not induce *CYP1A1* mRNAs, but almost fully antagonized TCDD in MCF7 WT cells. However, RES failed to antagonize DIM, but rather potentiated DIM-induced *CYP1A1* mRNA levels above those of DIM alone, similar to those of TCDD (Figure 10A).

Similar to that observed in MCF7 WT cells, 1 nM TCDD significantly increased *CYP1A1* mRNA levels in MDA-MB-231 WT cells (Figure 10B). In contrast to that observed in MCF7 WT cells, 10 μM DIM treatment resulted in a higher induction of *CYP1A1* mRNA levels (153%) compared to 1 nM TCDD (Figure 10B). RES treatment alone had no effect on *CYP1A1* levels, while its co-treatment with TCDD antagonized TCDD-induced increases in *CYP1A1* mRNA. In agreement with that observed in MCF7 cells, RES did not antagonize DIM-dependent increases in *CYP1A1* mRNA levels. DIM+RES co-treatment did not

significantly increase *CYP1A1* levels above those of DIM alone (Figure 10B). These data revealed that RES antagonized TCDD but not DIM-mediated AHR-dependent induction of *CYP1A1* mRNA levels.

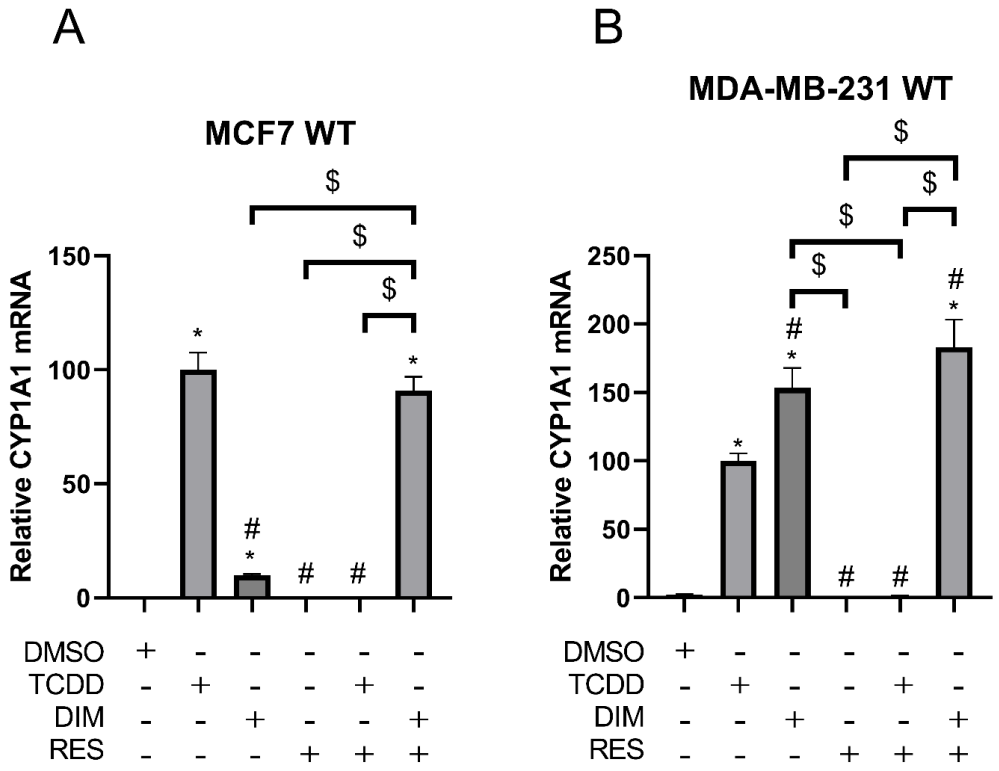

Figure 10. AHR agonists and antagonist affect the relative *CYP1A1* mRNA expression. **A** Expression of relative *CYP1A1* mRNA level in MCF7 WT cells. **B** Expression of relative *CYP1A1* mRNA level in MDA-MB-231 WT cells. MCF7 WT and MDA-MB-231 WT were treated for 24 hours with DMSO (control), 1 nM TCDD, 10 µM DIM, 10 µM RES, or a combination of these. Fold change was calculated using the ΔΔCT method and are presented as mean ± SEM of n=6 replicates normalized to 100% of the corresponding WT treated with TCDD. Significant differences were detected by one-way analysis of variance (ANOVA). * Significant differences compared to DMSO. # Significant differences compared to TCDD. $ Significant differences between the corresponding ligand treatments. Significance level was set to $p<0.05$.

To determine if the changes in *CYP1A1* mRNA were reflected in reciprocal changes in CYP1A1 activity in MCF7 WT and MDA-MB-231 WT cells, I measured the rate at which CYP1A1 converted ETX to resorufin, referred to as the EROD activity, after treatment with the different AHR ligands for 24 hours. TCDD, which was used as positive control in this assay, significantly increased EROD activity in both MCF7 WT (Figure 11A) and MDA-MB-231 WT cells

(Figure 11B). DIM treatment alone increased EROD activity in both cell lines, at a level of 23% and 26% that of TCDD in MCF7 WT and MDA-MB-231 WT cells, respectively. RES had no effect on EROD activity in MCF7 WT cells, but a significant increase was observed in MDA-MB-231 WT cells. In contrast to the RES-dependent potentiation of DIM induced *CYP1A1* mRNA levels observed in MCF7 WT cells, no additional increases above DIM alone were observed in CYP1A1 enzyme activity with the co-treatment (Figure 11A). In MDA-MB-231 WT cells, DIM+RES resulted in similar levels of EROD activity compared with DIM alone (Figure 11B). However, CYP1A1 enzyme activity was higher in both MCF7 WT cells and MDA-MB-231 WT cells upon co-treatment with DIM and RES compared with RES alone. TCDD+RES co-treatment was not examined in this assay.

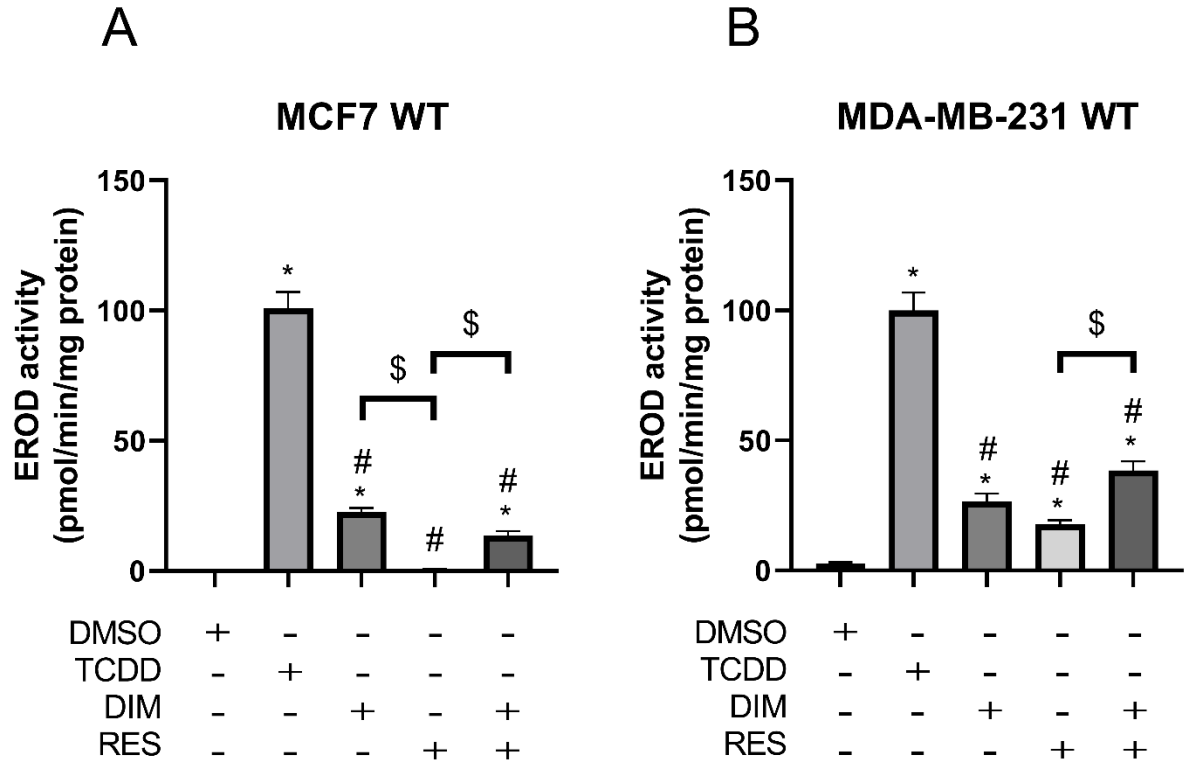

Figure 11. AHR ligand induced CYP1A1 enzymatic activity. (**A**) MCF7 WT cells and (**B**) MDA-MB-231 WT cells were treated 24 hours with DMSO (control), 10 nM TCDD, 10 µM DIM, 10 µM RES, or a combination of these, before the EROD assay was performed. Results are presented as mean ± SEM of n=8 replicates normalized to 100% of the corresponding WT treated with TCDD. Significant differences were detected by one-way analysis of variance (ANOVA). * Significant differences compared to DMSO. # Significant differences compared to TCDD. $ Significant differences between the corresponding ligand treatments. Significance level was set to $p<0.05$.

5.3 Proliferation of MCF7 and MDA-MB-231 cells are affected by DIM and RES

To establish if AHR knockout or its activation or inhibition affects proliferation of MCF7 or MDA-MB-231 cells I used a CellTiter-Glo® Luminescent Cell Viability Assay. MCF7 AHR^{ko} cells proliferated significantly less (26%) compared with MCF7 WT cells (Figure 12A). Treatment with DIM or RES alone had no significant effect on proliferation in MCF7 WT cells. However, co-treatment of DIM+RES significantly reduced proliferation of MCF7 WT cells (21% less) compared with DMSO (Figure 12B). This was also significantly less than treatment of either ligand alone. Similar to MCF7 WT cells, DIM alone had no effect of the proliferation rate of MCF7 AHR^{ko} cells (Figure 12C). In contrast, RES reduced the proliferation of MCF7 AHR^{ko} cells by 40% compared with DMSO. Similar findings were observed after DIM+RES co-treatment, but combination treatment was only significant from DIM treatment alone, and not from RES alone (Figure 12C).

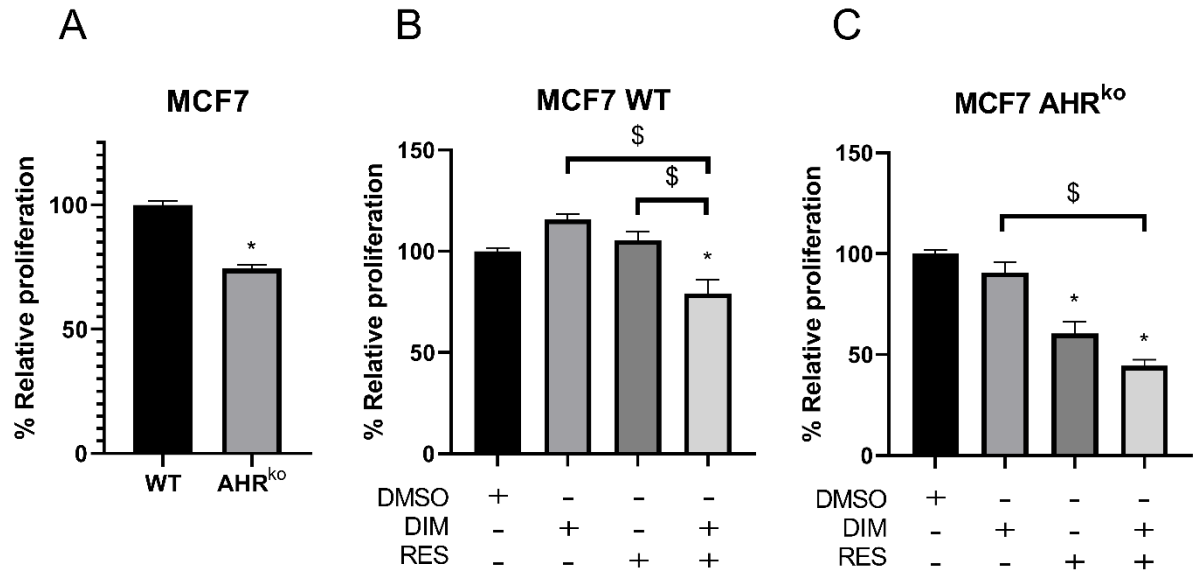

Figure 12. Proliferation of MCF7 WT and MCF7 AHR^{ko} cells. **A** Relative proliferation of MCF7 WT and MCF7 AHR^{ko} cells. Relative proliferation of (**B**) MCF7 WT or (**C**) MCF7 AHR^{ko} cells treated with DMSO, 10 µM DIM, 10 µM RES, or a combination of DIM and RES. The results are presented as mean ± SEM of n=12 replicates, and the y-axis is % proliferation after 72 hours relative to baseline normalized to 100% of the MCF7 WT (**A**) or the corresponding DMSO control (**B** and **C**). Significant differences were detected by Student's t-test and one-way analysis of variance (ANOVA). * Significant differences compared to MCF7 WT (**A**) or DMSO (**B** and **C**). $ Significant differences between the corresponding ligand treatments. Significance level was set to $p<0.05$.

In contrast to that observed in MCF7 cells, knockout of AHR did not affect cell proliferation in MDA-MB-231 cells (Figure 13A). Moreover, DIM treatment alone had no effect on the proliferation of MDA-MB-231 WT cells compared with DMSO. However, proliferation of MDA-MB-231 WT cells was significantly decreased by RES with 20%, which was further decreased by DIM+RES co-treatment (57 %) compared with DMSO (Figure 13B). The co-treatment also significantly reduced proliferation compared with treatment of either ligand alone. Treatment of MDA-MB-231 AHR^{ko} cells with DIM or RES alone or in combination significantly reduced their proliferation by 32%, 54% and 70%, respectively (Figure 13C). The co-treatment was also significantly different from treatment of DIM alone, but not RES. Collectively, these data suggest that the combination of DIM and RES together inhibits proliferation of MCF7 and MDA-MB-231 cells independently of AHR.

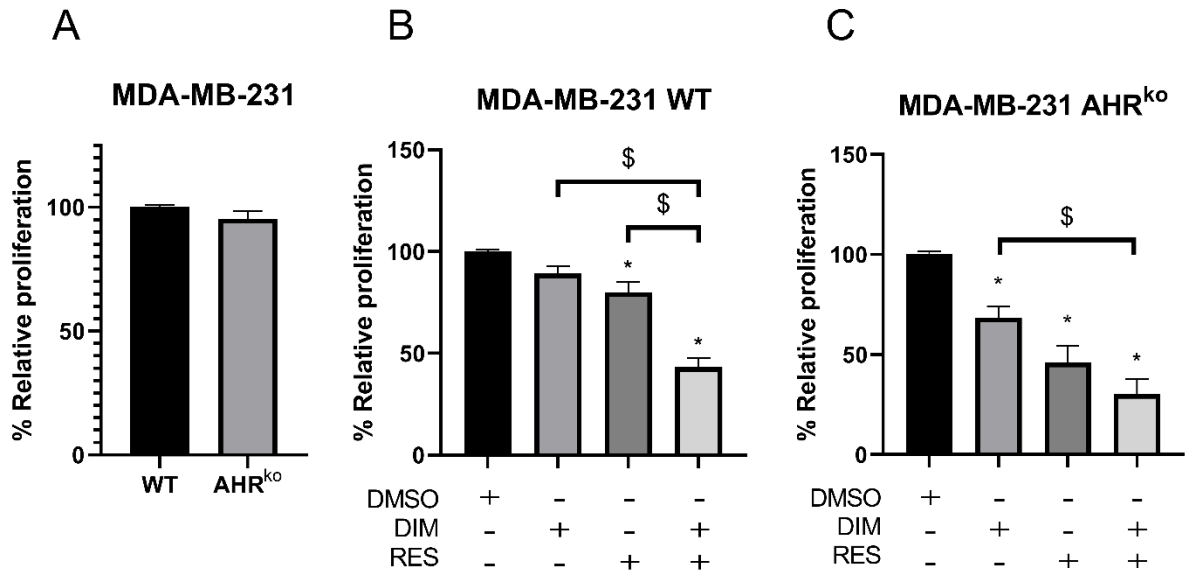

Figure 13. Proliferation of MDA-MB-231 WT and MDA-MB-231 AHR^{ko} cells. **A** Relative proliferation of MDA-MB-231 WT and MDA-MB-231 AHR^{ko} cells. Relative proliferation of (**B**) MDA-MB-231 WT or (**C**) MDA-MB-231 AHR^{ko} cells treated with DMSO, 10 µM DIM, 10 µM RES, or a combination of DIM and RES. The results are presented as mean ± SEM of n=12 replicates, and the y-axis is % proliferation after 72 hours relative to baseline normalized to 100% of the MDA-MB-231 WT (**A**) or the corresponding DMSO control (**B** and **C**). Significant differences were detected by Student's t-test and one-way analysis of variance (ANOVA). * Significant differences compared to MDA-MB-231 WT (**A**) or DMSO (**B** and **C**). $ Significant differences between the corresponding ligand treatments. Significance level was set to $p<0.05$.

5.4 Scratch assay

To examine the migrating properties of the cell lines, I performed scratch assays and compared the area of the scratch after 72 hours with the baseline area. Preliminary studies revealed that MCF7 cells did not migrate and were thus not further studied with scratch assays. MDA-MB-231 cells are more prone to migration than MCF7 cells due to their fibroblast looking structure and expression of vimentin (96).

MDA-MB-231 AHR^{ko} cells migrated significantly more than MDA-MB-231 WT cells. After 72 hours, 83% of the scratch was closed by MDA-MB-231 AHR^{ko} cells compared with 60% for MDA-MB-231 WT cells (Figure 14A and 14B).

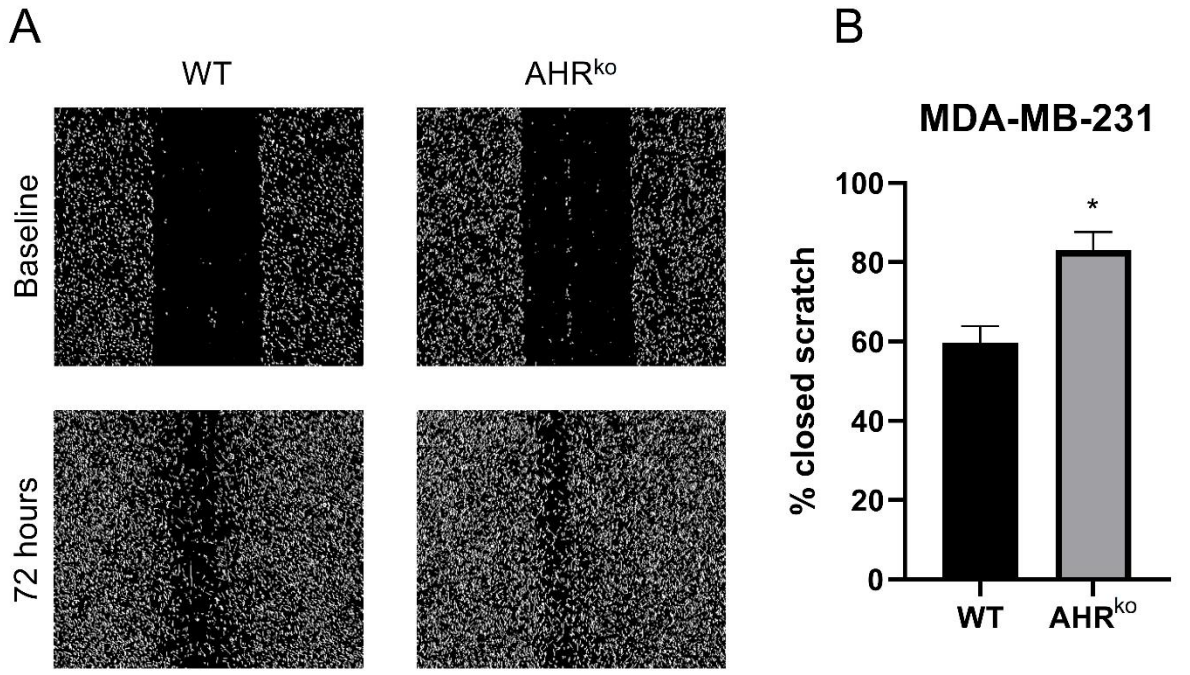

Figure 14. Migration of MDA-MB-231 WT and MDA-MB-231 AHR^{ko} cells. **A** Representative images of a scratch assay performed with MDA-MB-231 WT and MDA-MB-231 AHR^{ko} cells at baseline and after 72 hours. Images were made binary with the ImageJ software. **B** The % closure of the scratch of MDA-MB-231 WT and MDA-MB-231 AHR^{ko} cells. The results are after 72 hours after the scratch was made and are presented as mean ± SEM of n=9 replicates, three replicates of each cell line with three images per well for each replicate. Significant differences were detected by Student's t-test. * Significant differences compared to MDA-MB-231 WT. Significance level was set to $p<0.05$.

MDA-MB-231 WT cells treated with DIM migrated significantly less compared with DMSO, with only 34% closure of the scratch. RES alone had no effect on migration of MDA-MB-231

WT cells, but prevented the anti-migratory effects of DIM (Figure 15A). The co-treatment of DIM and RES led to significantly more migration compared to DIM treatment alone. MDA-MB-231 AHR^{ko} cells treated with DIM also migrated less than the DMSO control (Figure 15B). Similar to MDA-MB-231 WT cells, RES alone had no effect on migration of MDA-MB-231 AHR^{ko} cells, but prevented the anti-migratory effects of DIM (Figure 15B). MDA-MB-231 AHR^{ko} cells treated with RES or the co-treatment migrated significantly more than those treated with DIM.

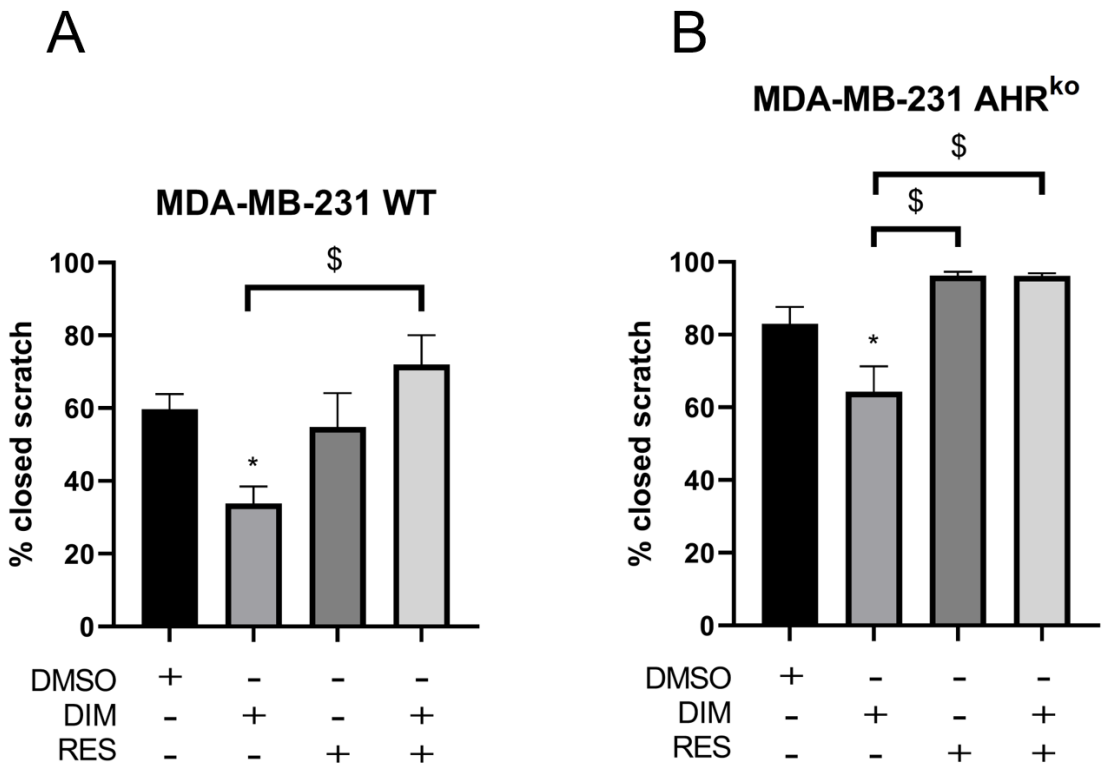

Figure 15. Migration of MDA-MB-231 WT and MDA-MB-231 AHR^{ko} cells treated with AHR ligands. The % closure of the scratch of (**A**) MDA-MB-231 WT cells and (**B**) MDA-MB-231 AHR^{ko} cells treated with DMSO, 10 µM DIM, 10 µM RES, or a combination of DIM and RES. The results are after 72 hours after the scratch was made and are presented as mean ± SEM of n=9 replicates, three replicates of each treatment with three images per well for each replicate. Significant differences were detected by one-way analysis of variance (ANOVA). * Significant differences compared to DMSO. $ Significant differences between the corresponding ligand treatments. Significance level was set to $p<0.05$.

5.5 Knockout of AHR downregulates E-cadherin expression and increase N-cadherin expression in MDA-MB-231 cells

Decreased expression of E-cadherin (*CDH1*) and increased expression of N-cadherin (*CDH2*) are hallmarks of EMT and are commonly called the "cadherin switch". As a potential mechanism to explain the scratch assay results, I examined the mRNA levels of *CDH1* and *CDH2*.

CDH1 mRNA levels were significantly lower in MDA-MB-231 AHR^{ko} cells compared with MDA-MB-231 WT cells (Figure 16A). In agreement with these findings, *CDH2* mRNA levels were significantly increased in MDA-MB-231 AHR^{ko} cells (Figure 16B). These findings support the results from the scratch assays revealing the increased migration of MDA-MB-231 AHR^{ko} cells compared with MDA-MB-231 WT cells.

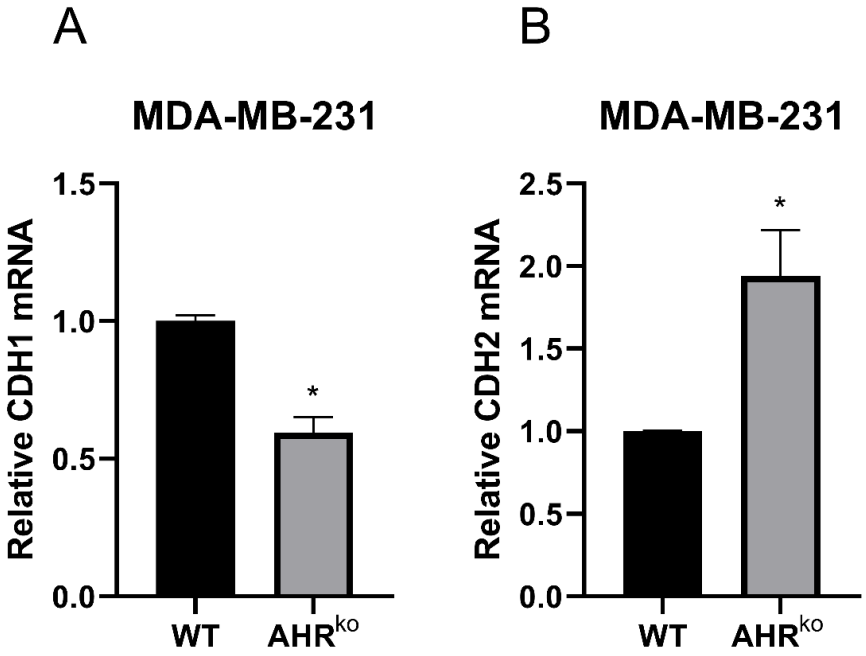

Figure 16. mRNA levels of (A) *CDH1* and (B) *CDH2* in MDA-MB-231 WT and MDA-MB-231 AHR^{ko} cells. Fold change was calculated using the ΔΔCT method and are presented as mean ± SEM of n=4 replicates normalized to 100% of the MDA-MB-231 WT cell line. Significant differences were detected by Student's t-test. * Significant difference compared to WT. Significance level was set to $p<0.05$.

I next examined the effect of AHR ligand treatment on *CDH1* and *CDH2* mRNA levels. Treatment with DIM or RES alone had no effect on *CDH1* mRNA level neither in MDA-MB-231 WT cells nor in MDA-MB-231 AHR^{ko} cells (Figure 17A and 17B). *CDH1* expression was significantly decreased with co-treatment of DIM and RES compared with

DMSO in MDA-MB-231 WT cells (Figure 17A), but had no effect in MDA-MB-231 AHR^{ko} cells (Figure 17B). *CDH2* mRNA levels were not affected by treatment of the AHR ligands alone nor in combination in both MDA-MB-231 WT and MDA-MB-231 AHR^{ko} cells (Figure 17C and 17D).

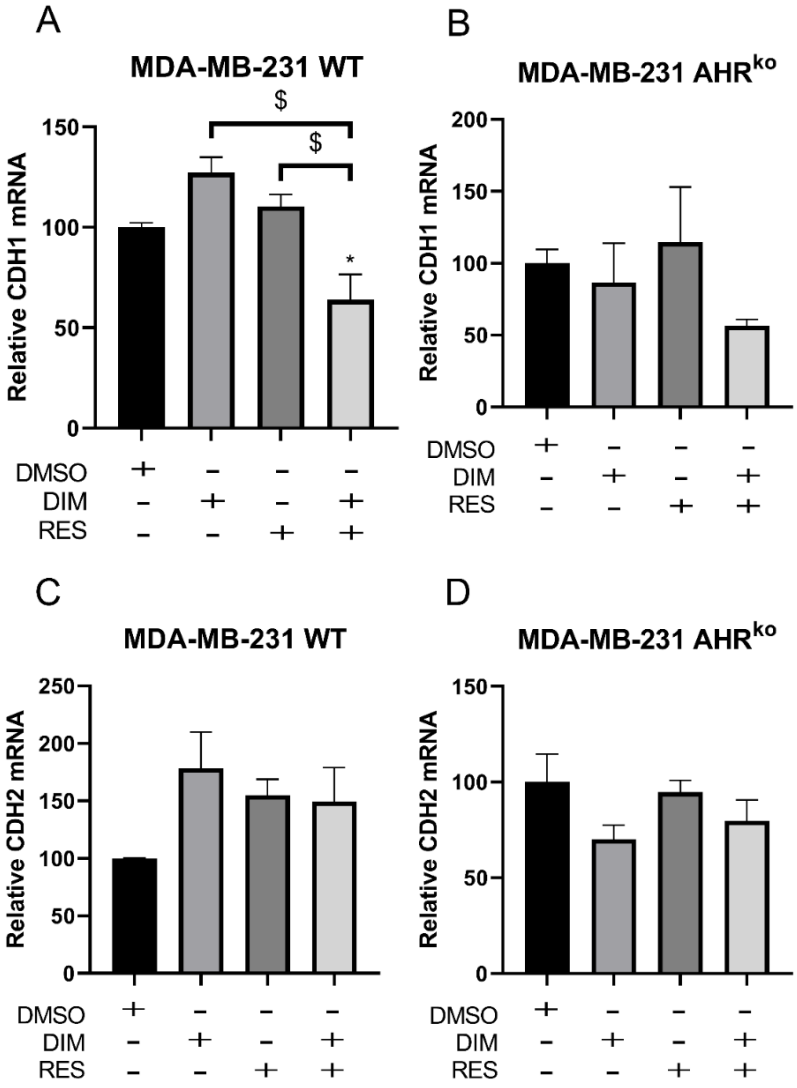

Figure 17. *CDH1* and *CDH2* mRNA level in MDA-MB-231 WT and MDA-MB-231 AHR^{ko} cells upon treatment with dietary AHR ligands. MDA-MB-231 WT and MDA-MB-231 AHR^{ko} cells were treated for 24 hours with DMSO, 10 µM DIM, 10 µM RES, or a combination of DIM and RES. *CDH1* mRNA level in (**A**) MDA-MB-231 WT and (**B**) MDA-MB-231 AHR^{ko} cells. *CDH2* mRNA level in (**C**) MDA-MB-231 WT and (**D**) MDA-MB-231 AHR^{ko} cells. Fold change was calculated using the ΔΔCT method and are presented as mean ± SEM of n=4 replicates normalized to 100% of the corresponding DMSO control. Significant differences were detected by one-way analysis of variance (ANOVA). * Significant differences compared to DMSO. $ Significant differences between the corresponding ligand treatments. Significance level was set to $p<0.05$.

6 Discussion

6.1 Methodological considerations

6.1.1 Gene editing approaches

Targeted gene editing approaches, like ZFN and CRISPR/Cas9, are relatively easy to perform to provide introduction of indels in a pooled cell population. However, it is somewhat more challenging to isolate cell clones where all copies of the gene of interest have indels resulting in frameshift mutations and the introduction of a premature stop codon, even after clonal dilution. This is exactly what we experienced with the MDA-MB-468 AHR^{ko} TO cell line, which after rigorous testing showed that the cell line had residual AHR activity as measured by TCDD-induced *CYP1A1* mRNA levels. DNA sequencing revealed that 1/20 independently sequenced clones had a deletion of 12 bp, removing amino acids at position 10 to 13 without altering the reading frame (Figure 5). Although western blotting did not clearly identify AHR protein, the presence of the AHR protein with a deletion of amino acids 10 to 13 most likely explains the residual AHR activity observed after TCDD treatment. Based on these findings I generated a MDA-MB-468 AHR^{ko} cell line by CRISPR/Cas9 as part of my thesis.

ZFN was used to generate MCF7 AHR^{ko} and MDA-MB-231 AHR^{ko} cells, while CRISPR/Cas9 was used to generate MDA-MB-468 AHR^{ko} cells. Even though the techniques are different, they ultimately result in a double-stranded DNA break. The cells repair double-stranded DNA breaks by either HDR or NHEJ. Since the wanted product was AHR knockout cell lines, we relied on error prone NHEJ DNA repair mechanisms. All of the indels created resulted in frameshift mutations, leading to premature stop codons in both the isolated ZFN and CRISPR/Cas9 AHR^{ko} cell lines. CRISPR/Cas9 is generally a more efficient and faster gene editing method than ZFN, in terms of design and implementation. However, the speed at which a gene edited cell line can be generated depends mostly on its proliferation rate. For example, MDA-MB-468 cells were transfected with the CRISPR/Cas9 plasmid during the first week of January 2021, but the isolated clones were not identified until mid-April. However, for other cell lines that proliferate more quickly, the lab has isolated and confirmed AHR^{ko} clones in as little as 4 weeks.

As with all gene editing techniques there are some inherent limitations. Although the ZFNs and sgRNAs are designed specific for exon 1 of AHR, we cannot exclude potential off-target effects such as the introduction of indels at other genomic locations in the cell lines. Unlike ZFN that require two proteins to bind and cut the DNA strand creating a double-stranded DNA break,

the CRISPR/Cas system is functional as a monomer, which increases potential off-target effects (97). However, using different types of Cas proteins, strategically engineered Cas proteins or improved sgRNA design methods can reduce off-target effects (98). In addition, the use of mutated Cas proteins that cause single-stranded DNA breaks, referred to as nickase activity, requires two Cas proteins each with their specific sgRNA to target the sequence of interest. These Cas nickases function in a similar manner to how ZFN proteins function by targeting each DNA strand resulting in a double-stranded DNA break. Thus, the double-stranded DNA break only occurs when both nickases bind in the correct location (98). One drawback with this approach is the need to design two sgRNAs for each target sequence, which could be problematic depending on the sequence.

Regardless of the gene editing approach used, off-target effects are a concern and a limitation of this technology. For example, it is possible that some of the effects observed in the different AHR^{ko} cells could be due to off-target mutations in genes involved in cell cycle progression or cell migration. Re-expressing AHR in the AHR^{ko} cells could be one approach to verify that the phenotypes observed are dependent on AHR. Moreover, whole cell genomic sequencing would be needed to determine the extent of off-target effects in the AHR^{ko} cells. This, however, is expensive and beyond the scope of this thesis.

6.1.2 Measurement of proliferation

The CellTiter-Glo® Luminescent Cell Viability Assay was used to measure the rate of MCF7 and MDA-MB-231 cell proliferation. The assay measures the luminescent signal created when luciferin is converted to oxyluciferin by the thermostable Ultra-Glo™ Recombinant Luciferase in the presence of ATP, O_2 and Mg^{2+} (99). The luminescence signal generated is proportionate to the amount of ATP present. The quantified ATP, which is a marker of metabolically active cells, is directly proportionate to numbers of viable cells. The CellTiter-Glo® Reagent lyses the cells when added, and consequently releases endogenous enzymes like ATPases. ATPases reduce the amount of ATP and could thereby interfere with the ATP measurement. However, the CellTiter-Glo® Reagent inhibits these ATPases, thus eliminating this pitfall (99).

The use of an Incucyte® real-time using live-cell imaging and analysis instrument would be an improved method to the end-point CellTiter-Glo assay. End-point assays do not take into account kinetics unless multiple time points are used, nor do they have the capability of making simultaneous measurements in a single well. However, an Incucyte® instrument can measure cell growth and proliferation in real time over several cell divisions using label-free cell counts

or cell confluence measurements. Unfortunately, there was an issue with one of the objectives of the Incucyte® in the department, so I was unable to use it for my thesis work.

6.1.3 Scratch assay as a measurement of migration

The scratch assay was performed on MDA-MB-231 cells by moving a 1000 µl pipette tip vertically at a 90° angle. It was not performed on MCF7 cells, since preliminary studies showed that they did not migrate. Since the scratch was made manually, the potential error of creating unequal areas of the scratch is of course present. To diminish this potential error, three images were taken of each well, to control for in-well area differences, in addition to three technical replicates of each cell line and ligand treatment. This results in a total of twelve images of each cell line and ligand treatment at both time points that were included in the analyses. The area of the scratch was initially measured every 24 hours for 120 hours; however, a substantial migration was observed after 72 hours, and I therefore decided on this time point to compare to the baseline area. Images taken after 72 hours were at approximately the corresponding area to the baseline images. Using the Incucyte®, and specifically the scratch wound migration and invasion assays for live-cell analysis, would have eliminated many of the limitations of the manual scratch assay I used. However as already mentioned, the Incucyte® instrument was unavailable and the Incucyte® woundmaker tool that is used to make the scratch would need to be purchased before the assay could be performed.

Alternatively, I could have used another measurement of migration, such as transwell migration assay. This assay uses a Boyden chamber that allows cells to migrate through a porous membrane. Migratory cells are then stained and counted. This allows for a more objective measurement of migratory cells. However, scratch assay is a much cheaper and easier assay to perform and was the assay of choice for this thesis.

6.2 Discussion of the results

AHR has an important role in xenobiotic metabolism; however, more recent research has shown that it also regulates cell cycle, cell homeostasis and tumor development and progression. AHR's role in tumorigenesis and specifically in breast cancer is complicated, as it is influenced by cell context and breast cancer subtype. AHR agonists like DIM, have been suggested as potential therapy for ER^+ breast cancer due to AHR's ability to negatively regulate ERα signaling (100). AHR loss or treatment with AHR antagonists like RES have been proposed for the treatment of TNBCs (45). DIM an RES have multiple cellular targets, activate diverse

signaling pathways, inhibit drug metabolizing enzyme activity and act as antioxidants, and many of their anti-cancer effects may be independent of AHR. Moreover, the constitutive role of AHR in breast cancer remains unclear as its loss promotes cell growth in some cell lines, while inhibiting cell growth of others (101-104).

6.2.1 Co-treatment with DIM and RES increased *CYP1A1* mRNA expression

I observed that MCF7 WT cells were more responsive to TCDD treatment in terms of induction of *CYP1A1* mRNA levels than MDA-MB-231 WT cells, which was in agreement with previous studies (105). The increase in *CYP1A1* mRNA levels above DMSO was greater after DIM treatment of MCF7 cells compared with MDA-MB-231 cells. These data show that level of activation of AHR signaling greatly differs between the cell lines, with MCF7 WT cells being more sensitive to AHR ligand induction than MDA-MB-231 WT cells.

Consistent with the previous work of the lab group, RES did not induce *CYP1A1* mRNA levels and acted as a potent antagonist of TCDD (95). Surprisingly, RES did not antagonize DIM in neither MCF7 WT cells nor in MDA-MB-231 WT cells. DIM is readily metabolized by many different CYP450 enzymes including CYP1A2 and CYP3A4. A previous report observed decreased metabolism of DIM when co-treated with the AHR antagonists, quercetin or RES, which correlated with decreased *CYP1A2* mRNA levels (106, 107). DIM also increases the levels of *CYP3A4* mRNA in a pregnane x receptor-dependent manner (108), while RES attenuates pregnane x receptor signaling (109). In addition, a RES metabolite generated by CYP3A4 forms an irreversible complex that inhibits CYP3A4 activity in both animal and human studies (109-114). Although not confirmed in this thesis, the impact of RES on CYP1A2 and CYP3A4 levels and activity would result in decreased metabolism of DIM. This would further lead to increased AHR activation. The increased *CYP1A1* mRNA levels observed in MCF7 WT but not MDA-MB-231 WT cells after DIM+RES co-treatment compared with DIM alone, suggest that RES inhibits DIM metabolism to a greater extent in MCF7 WT cells than in MDA-MB-231 WT cells.

6.2.2 CYP1A1 enzyme activity upon treatment with dietary AHR ligands

CYP1A1 has an important mechanism in xenobiotic and endogenous ligand metabolism, and it is essential in detoxifying many compounds. However, if overwhelmed CYP1A1 is also involved in the metabolic activation of procarcinogens like B[*a*]P. Although CYP1A1 contributes to the activation of procarcinogens, *Cyp1a1*-null mice die within 30 days following oral exposure to B[*a*]P, while WT mice survived with no sign of toxicity (115). This

demonstrate that CYP1A1's detoxifying role is more important than its role in generating reactive metabolites.

Since the *CYP1A1* mRNA levels were elevated upon co-treatment with DIM and RES, one would expect correlative changes in CYP1A1 enzymatic activity as measured by an EROD assay. Despite a significant increase in CYP1A1 enzymatic activity with the DIM+RES co-treatment, no increase above DIM alone was observed. RES has previously been reported to inhibit CYP1A1 enzymatic activity in an EROD assay, where the inhibiting effect of RES was proposed to be due to competitive binding (116). Since the EROD assay measures enzyme activity and not protein levels like in a western blot, it is unclear whether the lack of increase in CYP1A1 activity was due to reduced translation of the *CYP1A1* mRNA into protein or reduced CYP1A1 enzymatic activity in the co-treated samples.

6.2.3 The effect of AHR^{ko} on proliferation of MCF7 and MDA-MB-231 cells

To further elucidate the effect on proliferation of human breast cancer cells upon depletion of AHR, I performed the CellTiter-Glo assay. My data show that the loss of AHR expression reduces the proliferation of ER^+ MCF7 cells, but has no effect on the proliferation of TNBC MDA-MB-231 cells, which is in contrast to previous reports (75, 117). Several studies have investigated the effect of AHR knockout or AHR knockdown using RNA interference on MCF7 and MDA-MB-231 cell proliferation. However, the effects vary among different laboratories. AHR knockdown in MCF7 cells has been reported to decrease cell proliferation, which is in agreement with the findings of the current thesis (118). Others have reported increased proliferation of MCF7 cells after AHR knockdown compared to WT cells (119). The latter study used a sulforhodamine B assay to measure cell proliferation. This is a colorimetric assay in which sulforhodamine B binds basic amino acid residues of cellular proteins under slightly acidic conditions, before washing off excess dye. If not washed properly, the measurement of cell mass will either be over- or under-estimated, and the assay depends on a homologous cell suspension with minimal cell aggregates (120, 121). These discrepancies may also be due to small variations in MCF7 cell culturing among different labs or differences in knockdown strategies or approaches. It is important to mention that knockdown studies do not completely eliminate AHR protein levels, and it is possible that the level of AHR knockdown differed between the two research groups. For my studies, the AHR protein was knocked out without any residual activity that could confound the interpretation of the data.

In contrast to previous reports (75, 117), I observed no effect of AHR^{ko} on proliferation in ER^- MDA-MB-231 cells. A recent study by Vogel et al. (122) confirmed a pro-apoptotic effect of AHR^{ko} or AHRR overexpression in both MCF7 and MDA-MB-231 cells. AHRR overexpression accompanied with AHR^{ko} provided no further increase of apoptosis, suggesting the effect of AHRR depended on AHR. Inhibition of AHR by the antagonist carnosol reduces MCF7 and MDA-MB-231 cell proliferation (123). The same study also found an anti-proliferative effect upon CYP1A1 knockdown. They observed a G1 cell cycle arrest of both MCF7 and MDA-MB-231 cells upon CYP1A1 knockdown mediated in part by reduction of CCND1 levels, and a trend of reduction of CDK4 levels. This correlates with AHR's role in cell cycle progression through its interactions with CDK4 and CCND1 (60). Inactivated AHR mediates cell cycle progression by hyperphosphorylation of RB1. In the absence of AHR, the interaction with CDK4 and CCND1 is disrupted, suggesting the cell cycle is paused in the G1 phase. Treatment of MCF7 cells with insulin-like growth factor 2, significantly increases AHR binding to the promotor region of *CCND1*, resulting in increased CCND1 expression, which was reduced in AHR knockdown cells (118). This shows that CCND1 levels are regulated by AHR, suggesting that loss of AHR will reduce CCND1 expression, ultimately leading to RB1 hypophosphorylation and G1 cell cycle arrest.

Furthermore, *Ahr*-null MEFs have a slowed progression through G2/M phase and increased level of apoptosis compared to WT MEFs. Progression of the cell to M phase is regulated in part by the Cdc2/cyclin B kinase complex and Plk. *Ahr*-null MEFs express significantly less Cdc2 and Plk. These findings highlight that AHR has several roles in cell cycle progression, and that its loss would be expected to reduce cell proliferation as I observed in MCF7 cells. As previously described, activated AHR inhibits proliferation of ER^+ breast cancer cells by inhibiting ER signaling. The medium used in the proliferation assay was supplemented with 10% FBS which contains estrogen. Consequently, one would expect the loss of AHR in MCF7 cells to increase proliferation of the cell line due to increased ER signaling. However, the opposite was observed. This may be due to the diverse roles of AHR in the cell cycle, and that this effect surpasses the impact of AHR on ER signaling. However, AHR's role in cell proliferation is influenced by cell context, since I did not observe a similar effect in MDA-MB-231 cells.

6.2.4 Co-treatment of DIM and RES affected proliferation independent of AHR

Treatment with 20 µM DIM for 24 hours has been reported to inhibit proliferation and induce apoptosis in both MCF7 and MDA-MB-231 cells by decreasing the levels of CCND1 (124). A

formulated DIM with higher bioavailability has also been observed to decrease CCND1 levels by inhibiting nuclear translocation of β-catenin (44). Despite this, I did not observe any anti-proliferative effects of DIM on either MCF7 WT cells or MDA-MB-231 WT cells. This may be a result of the lesser concentration of DIM used in the proliferation assay compared with the above-mentioned study. DIM did not affect the proliferation of MCF7 AHR^{ko} cells, but reduced the proliferation of MDA-MB-231 AHR^{ko} cells. This shows that DIM reduces cell proliferation independently of AHR and ERα. We cannot, however, exclude that potential off-target or clonal selection effects in the MDA-MB-231 AHR^{ko} cells might impact this phenotype. This could be addressed by rescue experiments in which AHR could be transfected into the MDA-MB-231 AHR^{ko} cells to determine if its re-expression prevents the DIM-dependent reduction on cell proliferation.

RES treatment alone did not affect the proliferation of MCF7 WT cells, but significantly reduced that of MCF7 AHR^{ko} cells. As indicated above, we cannot exclude that potential off-target or clonal selection effects in the MCF7 AHR^{ko} cells influence this observation. RES treatment significantly decreased proliferation of MDA-MB-231 WT and MDA-MB-231 AHR^{ko} cells. This implies that the anti-proliferative effect of RES is independent of AHR and ERα. The anti-proliferative effect was enhanced with co-treatment with DIM in MDA-MB-231 WT cells, but not in MDA-MB-231 AHR^{ko} cells. A study investigating the anti-proliferative effects of RES on MDA-MB-231 cells observed a 60% reduction when cells were treated 4 hours daily for 6 days with 10 µM RES. This effect was enhanced to an 80% reduction of cell counts when treated 24 hours for 6 days with the same concentration (125). The 6 day treatment of RES increased the number of cells in S phase. Similar results have been observed in MCF7 cells, where RES dose-dependently reduced proliferation when treated with concentrations between 10-80 µM for 24, 48 and 96 hours (126). This study observed a significant reduction in proliferation with 24 hours treatment with 10 µM RES, and the proliferation significantly decreased with increasing concentrations of RES. The dose-dependency was most profound at 48 hours of treatment. Further examination of the effect of RES revealed a decrease of CCND1 when treated with RES for 48 hours in MCF7 cells (126).

6.2.5 AHR^{ko} increase migration of MDA-MB-231 cells

Tumor metastasis is a devastating potential outcome of breast cancer, which generally result in a poorer prognosis. To determine if AHR loss or AHR ligand treatment affects the migration of MDA-MB-231 cells as a model of metastasis, I performed a scratch assay. MDA-MB-231 AHR^{ko} cells migrated faster compared with MDA-MB-231 WT cells. Since AHR loss had no

effect on proliferation of MDA-MB-231 cells, the increased wound closure observed in MDA-MB-231 AHR^{ko} cells was not due to increased proliferation compared with MDA-MB-231 WT cells. In addition, the scratch assay was done in the presence of only 1% (v/v) FBS, which further reduces the potential of cell proliferation as a source of error.

In agreement with my findings, AHR knockdown in MDA-MB-231 cells by small interfering RNA increases invasion measured by transwell migration assay (77). Omeprazole is a selective AHR modulator that induce AHR activity without binding directly to AHR, and has been reported to exhibit anti-migratory effects on a glioblastoma cell line (127). MDA-MB-231 cells treated with omeprazole in combination with the AHR antagonists 3',4'-methoxy-α-naphthoflavone or 3'-methoxy-4'-nitroflavone exhibited increased invasiveness compared to treatment with omeprazole alone (77). Other studies report decreased migration and invasion after treatment with the AHR agonists TCDD or 6-methyl-1,3,8-trichlorodibenzofuran (78), or with Flavipin (128), implying that activated AHR protects against cell migration. In agreement with these observations, a study previously performed by the lab group observed decreased migration of neural stem cells in $TIPARP^{-/-}$ mice (129). As previously described, TIPARP inhibits AHR activity by ADP-ribosylation, and by knockout of TIPARP, the AHR activity is increased.

Ligand activated AHR downregulates expression of E-cadherin (72), and chromatin immunoprecipitation assay confirm that AHR binds the promotor region of E-cadherin in a TCDD-dependent manner, indicating that E-cadherin is a target gene of AHR (130). In agreement with these reports, I observed reduced *CDH1* mRNA levels in the MDA-MB-231 AHR^{ko} cell line compared with MDA-MB-231 WT cells. I also observed increased levels of *CDH2* mRNA in the MDA-MB-231 AHR^{ko} cell line, suggesting a further increase in the mesenchymal properties of MDA-MB-231 cells upon AHR loss, ultimately increasing their migratory potential.

6.2.6 DIM reduced migration of MDA-MB-231 cells independent of AHR

Previous studies have reported that many AHR agonists, including DIM, exhibit anti-migratory effects on MDA-MB-231 cells (77, 78, 128). I observed similar effects of DIM in my studies. However, DIM also reduced the migration of MDA-MB-231 AHR^{ko} cells, demonstrating that the anti-migratory effect of DIM is independent of AHR. Interestingly, co-treatment with RES prevented the anti-migratory effect of DIM, suggesting an interaction between DIM and RES that affect the migratory properties of the cells. This highlights a limitation of utilizing DIM or

RES in cancer treatment, since their effects are not limited to one receptor or mechanism, but rather include several cellular mechanisms, and potentially other compounds or therapeutic compounds, as observed with the DIM+RES co-treatment in MCF7 and MDA-MB-231 cells.

Other indole compounds, such as I3C and ICZ have previously been investigated for their effect on migration in MCF7 and MDA-MB-231 cells (131). Treatment with I3C and ICZ significantly reduced migration in MCF7 and MDA-MB-231 cells in a dose dependent manner, although they had a greater impact on MCF7 (131). This was associated with increased expression of E-cadherin in MCF7 cells, and reduced expression of the mesenchymal marker vimentin and of focal adhesion kinase (FAK), which has an important role in regulating cell motility. In the current thesis, no effect of DIM treatment was observed on E-cadherin expression in either cell line.

7 Conclusion

The aim of the current thesis was to investigate the effect of AHR loss or its inhibition on the proliferative and migratory properties of ER^+ and ER^- breast cancer cells, to further contribute to the knowledge of targeting AHR as a therapeutic approach.

Loss of AHR reduced proliferation of ER^+ MCF7 cells, but had no effect on proliferation of the TNBC cell line MDA-MB-231. Treatment of the dietary AHR agonist DIM did not affect cell proliferation in MCF7 WT cells, MCF7 AHR^{ko} cells, or MDA-MB-231 WT cells. However, DIM had an anti-proliferative effect on the MDA-MB-231 AHR^{ko} cell line, although it cannot be excluded that this effect was due to off-target effects of the ZFN gene targeting technology applied, since reintroduction of AHR was not performed as part of the current thesis. The dietary AHR antagonist RES had an anti-proliferative effect independent of AHR.

Loss of AHR expression in MDA-MB-231 cells increased their migratory properties, which was further supported by the expression of E-cadherin and N-cadherin. Loss of AHR resulted in a decrease of E-cadherin expression in addition to increased N-cadherin expression. Treatment with DIM resulted in decreased migration of both MDA-MB-231 WT cells and MDA-MB-231 AHR^{ko} cells. This effect was abolished by co-treatment with RES. Neither DIM nor RES had an effect on E-cadherin or N-cadherin expression.

Based on the results presented in this thesis, there is a context dependency on whether targeting AHR protects against breast cancer progression or not. Loss of AHR has a protective effect in ER^+ MCF7 cells; however, it increases migration of MDA-MB-231 cells. The effect of DIM and RES on proliferation and migration of MCF7 and MDA-MB-231 cells were independent of AHR, suggesting that other regulatory mechanisms are involved. The role of AHR in tumor progression is complex and context dependent. Subsequently, more studies are needed to fully elucidate and understand the potential of AHR as a therapeutic target for treatment of breast cancer.

8 Future directions

The CRISPR/Cas9 generated MDA-MB-468 AHR^{ko} cell line will provide insight on how AHR^{ko} affects TNBCs with different properties. This cell line expresses epidermal growth factor receptors and display a less mesenchymal phenotype than MDA-MB-231 cells. Therefore, the effect of AHR^{ko} on proliferation and migration might differ from what was observed in MDA-MB-231 cells. Furthermore, different methods to investigate proliferation and migration, like Incucyte and transwell migration assay, will provide higher quality measurements and more in-depth analyses. Investigation of AHR^{ko} on cell cycle, apoptosis and DNA damage would elucidate the anti-proliferative observation in MCF7 cells. The effect of RES on cell cycle progression and apoptosis would also be of interest.

In vitro studies with isolated cells in culture do not provide insight into the mechanisms affecting cancer cells in context with tumor microenvironment and in living organisms. The current thesis has not examined the effect of AHR loss or ligand treatment in breast cancer cells in the presence of the immune system. AHR has been observed to promote evasion of the immune system of tumor cells through activation by KYN. This is an important aspect to consider when developing AHR targeting therapies. Co-culture assays with breast cancer and immune cells would provide further insight on how these interactions affect tumor growth. In addition, syngeneic mouse model studies where AHR^{ko} cancer cells could be injected into recipient mice with an intact immune system will be important in determining the effect *in vivo*.

There is currently an ongoing phase I clinical trial by Bayer Pharmaceuticals investigating the effect of an AHR antagonist (BAY2416964) on the tumor development in patients with advanced solid tumors as an immunotherapy. The results of this trial will be of major importance as to whether targeting AHR is an effective and safe treatment for patients with advanced and severe cancers.

8 References

1. International Agency of Research on Cancer (IARC). Global Cancer Observatory Cancer Today, Global Cancer Observatory Cancer Today, [updated December 2020; cited 01.02.2021. Available from: https://gco.iarc.fr/today/online-analysis-multi-bars?v=2020&mode=cancer&mode_population=countries&population=900&populations=900&key=total&sex=0&cancer=39&type=0&statistic=5&prevalence=0&population_group=0&ages_group%5B%5D=0&ages_group%5B%5D=17&nb_items=10&group_cancer=1&include_nmsc=1&include_nmsc_other=1&type_multiple=%257B%2522inc%2522%253Atrue%252C%2522mort%2522%253Afalse%252C%2522prev%2522%253Afalse%257D&orientation=horizontal&type_sort=0&type_nb_items=%257B%2522top%2522%253Atrue%252C%2522bottom%2522%253Afalse%257D.
2. International Agency of Research on Cancer (IARC), Latest global cancer data: Cancer burden rises to 19.3 million new cases and 10.0 million cancer deaths in 2020, Number 292 [press release]. 15. December 2020.
3. Waks AG, Winer EP. Breast Cancer Treatment: A Review. Jama. 2019;321(3):288-300.
4. Shagufta, Ahmad I. Tamoxifen a pioneering drug: An update on the therapeutic potential of tamoxifen derivatives. European Journal of Medicinal Chemistry. 2018;143:515-31.
5. Verma S, Joy AA, Rayson D, McLeod D, Brezden-Masley C, Boileau J-F, et al. HER story: the next chapter in HER-2-directed therapy for advanced breast cancer. Oncologist. 2013;18(11):1153-66.
6. Williams C, Lin C-Y. Oestrogen receptors in breast cancer: basic mechanisms and clinical implications. Ecancermedicalscience. 2013;7:370-.
7. Papoutsi Z, Zhao C, Putnik M, Gustafsson J-Å, Dahlman-Wright K. Binding of estrogen receptor α/β heterodimers to chromatin in MCF-7 cells. Journal of Molecular Endocrinology. 2009;43(2):65-72.
8. Leygue E, Murphy LC. A bi-faceted role of estrogen receptor β in breast cancer. Endocrine-Related Cancer. 2013;20(3):R127-R39.
9. The National Health Service (NHS). Treatment, breast cancer in women, [updated 28.10.2019; cited 25.04.2021. Available from: https://www.nhs.uk/conditions/breast-cancer/treatment/.
10. Fisher B, Costantino JP, Wickerham DL, Redmond CK, Kavanah M, Cronin WM, et al. Tamoxifen for prevention of breast cancer: report of the National Surgical Adjuvant Breast and Bowel Project P-1 Study. J Natl Cancer Inst. 1998;90(18):1371-88.
11. Chang M. Tamoxifen resistance in breast cancer. Biomol Ther (Seoul). 2012;20(3):256-67.
12. Ignatov A, Ortmann O. Endocrine Risk Factors of Endometrial Cancer: Polycystic Ovary Syndrome, Oral Contraceptives, Infertility, Tamoxifen. Cancers. 2020;12(7):1766.
13. Derakhshani A, Rezaei Z, Safarpour H, Sabri M, Mir A, Sanati MA, et al. Overcoming trastuzumab resistance in HER2-positive breast cancer using combination therapy. Journal of Cellular Physiology. 2020;235(4):3142-56.
14. The National Health Service (NHS). Herceptin (trastuzumab), [updated 12.11.2019; cited 25.04.2021. Available from: https://www.nhs.uk/conditions/herceptin/.

15. Sengupta PP, Northfelt DW, Gentile F, Zamorano JL, Khandheria BK. Trastuzumab-Induced Cardiotoxicity: Heart Failure at the Crossroads. Mayo Clinic Proceedings. 2008;83(2):197-203.
16. Al-Dasooqi N, Bowen JM, Gibson RJ, Sullivan T, Lees J, Keefe DM. Trastuzumab induces gastrointestinal side effects in HER2-overexpressing breast cancer patients. Invest New Drugs. 2009;27(2):173-8.
17. Fan W, Chang J, Fu P. Endocrine therapy resistance in breast cancer: current status, possible mechanisms and overcoming strategies. Future Med Chem. 2015;7(12):1511-9.
18. Le Beau MM, Carver LA, Espinosa IR, Schmidt JV, Bradfield CA. Chromosomal localization of the human AHR locus encoding the structural gene for the Ah receptor to 7p21→p15. Cytogenetic and Genome Research. 1994;66(3):172-6.
19. Matthews J. Chapter 7 Aryl Hydrocarbon Receptor Targeted by Xenobiotic Compounds and Dietary Phytochemicals. Hormone-Disruptive Chemical Contaminants in Food: The Royal Society of Chemistry; 2012. p. 115-35.
20. Hahn ME. Aryl hydrocarbon receptors: diversity and evolution11Invited review for Chemico-Biological Interactions. Chemico-Biological Interactions. 2002;141(1):131-60.
21. Jiang Y-z, Wang K, Fang R, Zheng J. Expression of aryl hydrocarbon receptor in human placentas and fetal tissues. J Histochem Cytochem. 2010;58(8):679-85.
22. Sato S, Shirakawa H, Tomita S, Ohsaki Y, Haketa K, Tooi O, et al. Low-dose dioxins alter gene expression related to cholesterol biosynthesis, lipogenesis, and glucose metabolism through the aryl hydrocarbon receptor-mediated pathway in mouse liver. Toxicology and Applied Pharmacology. 2008;229(1):10-9.
23. Poland A, Glover E, Kende AS. Stereospecific, high affinity binding of 2,3,7,8-tetrachlorodibenzo-p-dioxin by hepatic cytosol. Evidence that the binding species is receptor for induction of aryl hydrocarbon hydroxylase. J Biol Chem. 1976;251(16):4936-46.
24. Steenland K, Bertazzi P, Baccarelli A, Kogevinas M. Dioxin revisited: developments since the 1997 IARC classification of dioxin as a human carcinogen. Environ Health Perspect. 2004;112(13):1265-8.
25. Murray IA, Patterson AD, Perdew GH. Aryl hydrocarbon receptor ligands in cancer: friend and foe. Nature reviews Cancer. 2014;14(12):801-14.
26. Kerkvliet NI. AHR-mediated immunomodulation: the role of altered gene transcription. Biochem Pharmacol. 2009;77(4):746-60.
27. Safe S, Cheng Y, Jin U-H. The Aryl Hydrocarbon Receptor (AhR) as a Drug Target for Cancer Chemotherapy. Current opinion in toxicology. 2017;2:24-9.
28. Kazlauskas A, Poellinger L, Pongratz I. Evidence that the co-chaperone p23 regulates ligand responsiveness of the dioxin (Aryl hydrocarbon) receptor. J Biol Chem. 1999;274(19):13519-24.
29. Baker JR, Sakoff JA, McCluskey A. The aryl hydrocarbon receptor (AhR) as a breast cancer drug target. Med Res Rev. 2020;40(3):972-1001.
30. Hankinson O. Role of coactivators in transcriptional activation by the aryl hydrocarbon receptor. Archives of Biochemistry and Biophysics. 2005;433(2):379-86.
31. Avilla MN, Malecki KMC, Hahn ME, Wilson RH, Bradfield CA. The Ah Receptor: Adaptive Metabolism, Ligand Diversity, and the Xenokine Model. Chemical Research in Toxicology. 2020;33(4):860-79.

32. Pollenz RS. The mechanism of AH receptor protein down-regulation (degradation) and its impact on AH receptor-mediated gene regulation. Chemico-Biological Interactions. 2002;141(1):41-61.
33. Vogel CFA, Haarmann-Stemmann T. The aryl hydrocarbon receptor repressor - More than a simple feedback inhibitor of AhR signaling: Clues for its role in inflammation and cancer. Curr Opin Toxicol. 2017;2:109-19.
34. Matthews J. AHR toxicity and signaling: Role of TIPARP and ADP-ribosylation. Current Opinion in Toxicology. 2017;2:50-7.
35. MacPherson L, Tamblyn L, Rajendra S, Bralha F, McPherson JP, Matthews J. 2,3,7,8-Tetrachlorodibenzo-p-dioxin poly(ADP-ribose) polymerase (TiPARP, ARTD14) is a mono-ADP-ribosyltransferase and repressor of aryl hydrocarbon receptor transactivation. Nucleic Acids Res. 2013;41(3):1604-21.
36. Androutsopoulos VP, Tsatsakis AM, Spandidos DA. Cytochrome P450 CYP1A1: wider roles in cancer progression and prevention. BMC Cancer. 2009;9(1):187.
37. Jane Higdon, Victoria Drake, Barbara Delage, David Williams. Indole-3-Carbinol, Linus Pauling Institute, [updated July 2017; cited 25.04.2021. Available from: https://lpi.oregonstate.edu/mic/dietary-factors/phytochemicals/indole-3-carbinol.
38. Chen I, McDougal A, Wang F, Safe S. Aryl hydrocarbon receptor-mediated antiestrogenic and antitumorigenic activity of diindolylmethane. Carcinogenesis. 1998;19(9):1631-9.
39. Thomson CA, Ho E, Strom MB. Chemopreventive properties of 3,3'-diindolylmethane in breast cancer: evidence from experimental and human studies. Nutr Rev. 2016;74(7):432-43.
40. Okino ST, Pookot D, Basak S, Dahiya R. Toxic and chemopreventive ligands preferentially activate distinct aryl hydrocarbon receptor pathways: implications for cancer prevention. Cancer prevention research (Philadelphia, Pa). 2009;2(3):251-6.
41. Huang Z, Zuo L, Zhang Z, Liu J, Chen J, Dong L, et al. 3,3′-Diindolylmethane decreases VCAM-1 expression and alleviates experimental colitis via a BRCA1-dependent antioxidant pathway. Free Radical Biology and Medicine. 2011;50(2):228-36.
42. Li Y, Kong D, Ahmad A, Bao B, Sarkar FH. Antioxidant function of isoflavone and 3,3'-diindolylmethane: are they important for cancer prevention and therapy? Antioxid Redox Signal. 2013;19(2):139-50.
43. Kong D, Banerjee S, Huang W, Li Y, Wang Z, Kim H-RC, et al. Mammalian target of rapamycin repression by 3,3'-diindolylmethane inhibits invasion and angiogenesis in platelet-derived growth factor-D-overexpressing PC3 cells. Cancer Res. 2008;68(6):1927-34.
44. Li Y, Wang Z, Kong D, Murthy S, Dou QP, Sheng S, et al. Regulation of FOXO3a/beta-catenin/GSK-3beta signaling by 3,3'-diindolylmethane contributes to inhibition of cell proliferation and induction of apoptosis in prostate cancer cells. J Biol Chem. 2007;282(29):21542-50.
45. Ko J-H, Sethi G, Um J-Y, Shanmugam MK, Arfuso F, Kumar AP, et al. The Role of Resveratrol in Cancer Therapy. Int J Mol Sci. 2017;18(12):2589.
46. Catalgol B, Batirel S, Taga Y, Ozer NK. Resveratrol: French paradox revisited. Front Pharmacol. 2012;3:141-.
47. Casper RF, Quesne M, Rogers IM, Shirota T, Jolivet A, Milgrom E, et al. Resveratrol has antagonist activity on the aryl hydrocarbon receptor: implications for prevention of dioxin toxicity. Mol Pharmacol. 1999;56(4):784-90.

48. Lee GA, Hwang KA, Choi KC. Roles of Dietary Phytoestrogens on the Regulation of Epithelial-Mesenchymal Transition in Diverse Cancer Metastasis. Toxins (Basel). 2016;8(6).
49. Bianco NR, Chaplin LJ, Montano MM. Differential induction of quinone reductase by phytoestrogens and protection against oestrogen-induced DNA damage. Biochem J. 2005;385(Pt 1):279-87.
50. Yang X, Solomon S, Fraser LR, Trombino AF, Liu D, Sonenshein GE, et al. Constitutive regulation of CYP1B1 by the aryl hydrocarbon receptor (AhR) in pre-malignant and malignant mammary tissue. J Cell Biochem. 2008;104(2):402-17.
51. Jeschke U, Zhang X, Kuhn C, Jalaguier S, Colinge J, Pfender K, et al. The Prognostic Impact of the Aryl Hydrocarbon Receptor (AhR) in Primary Breast Cancer Depends on the Lymph Node Status. Int J Mol Sci. 2019;20(5):1016.
52. Stephen Safe and Mark Wormke. Inhibitory Aryl Hydrocarbon Receptor−Estrogen Receptor α Cross-Talk and Mechanisms of Action. Chem Res Toxicol.2003.
53. Matthews J, Gustafsson J-A. Estrogen receptor and aryl hydrocarbon receptor signaling pathways. Nucl Recept Signal. 2006;4:e016-e.
54. Ohtake F, Baba A, Takada I, Okada M, Iwasaki K, Miki H, et al. Dioxin receptor is a ligand-dependent E3 ubiquitin ligase. Nature. 2007;446(7135):562-6.
55. Lee AJ, Cai MX, Thomas PE, Conney AH, Zhu BT. Characterization of the oxidative metabolites of 17beta-estradiol and estrone formed by 15 selectively expressed human cytochrome p450 isoforms. Endocrinology. 2003;144(8):3382-98.
56. Göttel M, Le Corre L, Dumont C, Schrenk D, Chagnon M-C. Estrogen receptor α and aryl hydrocarbon receptor cross-talk in a transfected hepatoma cell line (HepG2) exposed to 2,3,7,8-tetrachlorodibenzo-p-dioxin. Toxicol Rep. 2014;1:1029-36.
57. Rosen EM, Fan S, Pestell RG, Goldberg ID. BRCA1 gene in breast cancer. J Cell Physiol. 2003;196(1):19-41.
58. Romagnolo DF, Papoutsis AJ, Laukaitis C, Selmin OI. Constitutive expression of AhR and BRCA-1 promoter CpG hypermethylation as biomarkers of ERα-negative breast tumorigenesis. BMC Cancer. 2015;15(1):1026.
59. Kang HJ, Kim HJ, Kim SK, Barouki R, Cho C-H, Khanna KK, et al. BRCA1 Modulates Xenobiotic Stress-inducible Gene Expression by Interacting with ARNT in Human Breast Cancer Cells *. Journal of Biological Chemistry. 2006;281(21):14654-62.
60. Barhoover MA, Hall JM, Greenlee WF, Thomas RS. Aryl hydrocarbon receptor regulates cell cycle progression in human breast cancer cells via a functional interaction with cyclin-dependent kinase 4. Mol Pharmacol. 2010;77(2):195-201.
61. John K, Lahoti TS, Wagner K, Hughes JM, Perdew GH. The Ah receptor regulates growth factor expression in head and neck squamous cell carcinoma cell lines. Mol Carcinog. 2014;53(10):765-76.
62. Kubli SP, Bassi C, Roux C, Wakeham A, Göbl C, Zhou W, et al. AhR controls redox homeostasis and shapes the tumor microenvironment in BRCA1-associated breast cancer. Proceedings of the National Academy of Sciences. 2019;116(9):3604.
63. Wang CK, Chang H, Chen PH, Chang JT, Kuo YC, Ko JL, et al. Aryl hydrocarbon receptor activation and overexpression upregulated fibroblast growth factor-9 in human lung adenocarcinomas. International journal of cancer. 2009;125(4):807-15.
64. Kawajiri K, Kobayashi Y, Ohtake F, Ikuta T, Matsushima Y, Mimura J, et al. Aryl hydrocarbon receptor suppresses intestinal carcinogenesis in Apc^{Min/+} mice with natural ligands. Proceedings of the National Academy of Sciences. 2009;106(32):13481.

65. Puga A, Barnes SJ, Dalton TP, Chang C-y, Knudsen ES, Maier MA. Aromatic Hydrocarbon Receptor Interaction with the Retinoblastoma Protein Potentiates Repression of E2F-dependent Transcription and Cell Cycle Arrest*. Journal of Biological Chemistry. 2000;275(4):2943-50.
66. Elferink CJ, Ge NL, Levine A. Maximal aryl hydrocarbon receptor activity depends on an interaction with the retinoblastoma protein. Mol Pharmacol. 2001;59(4):664-73.
67. Kolluri SK, Weiss C, Koff A, Göttlicher M. p27(Kip1) induction and inhibition of proliferation by the intracellular Ah receptor in developing thymus and hepatoma cells. Genes Dev. 1999;13(13):1742-53.
68. Elizondo G, Fernandez-Salguero P, Sheikh MS, Kim GY, Fornace AJ, Lee KS, et al. Altered cell cycle control at the G(2)/M phases in aryl hydrocarbon receptor-null embryo fibroblast. Mol Pharmacol. 2000;57(5):1056-63.
69. Terashima J, Tachikawa C, Kudo K, Habano W, Ozawa S. An aryl hydrocarbon receptor induces VEGF expression through ATF4 under glucose deprivation in HepG2. BMC Mol Biol. 2013;14:27.
70. Thiery JP, Acloque H, Huang RYJ, Nieto MA. Epithelial-Mesenchymal Transitions in Development and Disease. Cell. 2009;139(5):871-90.
71. Lamouille S, Xu J, Derynck R. Molecular mechanisms of epithelial–mesenchymal transition. Nature Reviews Molecular Cell Biology. 2014;15(3):178-96.
72. Dietrich C, Kaina B. The aryl hydrocarbon receptor (AhR) in the regulation of cell-cell contact and tumor growth. Carcinogenesis. 2010;31:1319-28.
73. Diry M, Tomkiewicz C, Koehle C, Coumoul X, Bock KW, Barouki R, et al. Activation of the dioxin/aryl hydrocarbon receptor (AhR) modulates cell plasticity through a JNK-dependent mechanism. Oncogene. 2006;25(40):5570-4.
74. Tsai CL, Li HP, Lu YJ, Hsueh C, Liang Y, Chen CL, et al. Activation of DNA methyltransferase 1 by EBV LMP1 Involves c-Jun NH(2)-terminal kinase signaling. Cancer Res. 2006;66(24):11668-76.
75. Goode GD, Ballard BR, Manning HC, Freeman ML, Kang Y, Eltom SE. Knockdown of aberrantly upregulated aryl hydrocarbon receptor reduces tumor growth and metastasis of MDA-MB-231 human breast cancer cell line. International journal of cancer. 2013;133(12):2769-80.
76. Shadboorestan A, Tarfiei GA, Montazeri H, Sepand MR, Zangooei M, Khedri A, et al. Invasion and migration of MDA-MB-231 cells are inhibited by block of AhR and NFAT: role of AhR/NFAT1/β4 integrin signaling. J Appl Toxicol. 2019;39(2):375-84.
77. Jin UH, Lee SO, Pfent C, Safe S. The aryl hydrocarbon receptor ligand omeprazole inhibits breast cancer cell invasion and metastasis. BMC Cancer. 2014;14:498.
78. Zhang S, Kim K, Jin UH, Pfent C, Cao H, Amendt B, et al. Aryl hydrocarbon receptor agonists induce microRNA-335 expression and inhibit lung metastasis of estrogen receptor negative breast cancer cells. Mol Cancer Ther. 2012;11(1):108-18.
79. Donovan MG, Selmin OI, Romagnolo DF. Aryl Hydrocarbon Receptor Diet and Breast Cancer Risk. Yale J Biol Med. 2018;91(2):105-27.
80. Prendergast GC, Malachowski WP, DuHadaway JB, Muller AJ. Discovery of IDO1 Inhibitors: From Bench to Bedside. Cancer Res. 2017;77(24):6795-811.
81. Shergold AL, Millar R, Nibbs RJB. Understanding and overcoming the resistance of cancer to PD-1/PD-L1 blockade. Pharmacol Res. 2019;145:104258.
82. Narasimhan S, Stanford Zulick E, Novikov O, Parks AJ, Schlezinger JJ, Wang Z, et al. Towards Resolving the Pro- and Anti-Tumor Effects of the Aryl Hydrocarbon Receptor. Int J Mol Sci. 2018;19(5).

83. Kenison JE, Wang Z, Yang K, Snyder M, Quintana FJ, Sherr DH. The aryl hydrocarbon receptor suppresses immunity to oral squamous cell carcinoma through immune checkpoint regulation. Proceedings of the National Academy of Sciences. 2021;118(19):e2012692118.
84. Carroll D. Genome Editing: Past, Present, and Future. Yale J Biol Med. 2017;90(4):653-9.
85. Gaj T, Sirk SJ, Shui S-L, Liu J. Genome-Editing Technologies: Principles and Applications. Cold Spring Harb Perspect Biol. 2016;8(12):a023754.
86. Le Rhun A, Escalera-Maurer A, Bratovič M, Charpentier E. CRISPR-Cas in Streptococcus pyogenes. RNA Biol. 2019;16(4):380-9.
87. Khalil AM. The genome editing revolution: review. J Genet Eng Biotechnol. 2020;18(1):68.
88. Jinek M, Chylinski K, Fonfara I, Hauer M, Doudna JA, Charpentier E. A programmable dual-RNA-guided DNA endonuclease in adaptive bacterial immunity. Science. 2012;337(6096):816-21.
89. Vasbinder MM GJ, Abo RP, Kunii K, Kuplast-Barr KG, Gui B, Lu AZ, Swinger KK, Wigle TJ, Blackwell DJ, Majer CR, Ren Y, Niepel M, Varsamis ZA, Nayak SP, Bamberg E, Mo JR, Church WD, Song J, Utley L, Rao PE, Mitchison TJ, Kuntz KW, Richon VM, Keilhack H. RBN-2397 – A First-in-Class PARP7 Inhibitor Targeting a Newly Discovered Cancer Vulnerability in Stress-Signaling Pathways. April 2020 American Association of Cancer Research (AACR) Virtual Annual Meeting I.
90. Ahmed S, Wang A, Celius T, Matthews J. Zinc finger nuclease-mediated knockout of AHR or ARNT in human breast cancer cells abolishes basal and ligand-dependent regulation of CYP1B1 and differentially affects estrogen receptor α transactivation. Toxicol Sci. 2014;138(1):89-103.
91. Suarez-Arnedo A, Torres Figueroa F, Clavijo C, Arbeláez P, Cruz JC, Muñoz-Camargo C. An image J plugin for the high throughput image analysis of in vitro scratch wound healing assays. PloS one. 2020;15(7):e0232565-e.
92. Denison MS, Nagy SR. Activation of the aryl hydrocarbon receptor by structurally diverse exogenous and endogenous chemicals. Annu Rev Pharmacol Toxicol. 2003;43:309-34.
93. Leong H, Firestone GL, Bjeldanes LF. Cytostatic effects of 3,3′-diindolylmethane in human endometrial cancer cells result from an estrogen receptor-mediated increase in transforming growth factor-α expression. Carcinogenesis. 2001;22(11):1809-17.
94. Sanderson JT, Slobbe L, Lansbergen GW, Safe S, van den Berg M. 2,3,7,8-Tetrachlorodibenzo-p-dioxin and diindolylmethanes differentially induce cytochrome P450 1A1, 1B1, and 19 in H295R human adrenocortical carcinoma cells. Toxicol Sci. 2001;61(1):40-8.
95. Macpherson L, Matthews J. Inhibition of aryl hydrocarbon receptor-dependent transcription by resveratrol or kaempferol is independent of estrogen receptor α expression in human breast cancer cells. Cancer letters. 2010;299(2):119-29.
96. Thompson EW, Paik S, Brünner N, Sommers CL, Zugmaier G, Clarke R, et al. Association of increased basement membrane invasiveness with absence of estrogen receptor and expression of vimentin in human breast cancer cell lines. J Cell Physiol. 1992;150(3):534-44.
97. Koo T, Lee J, Kim J-S. Measuring and Reducing Off-Target Activities of Programmable Nucleases Including CRISPR-Cas9. Mol Cells. 2015;38(6):475-81.

98. Naeem M, Majeed S, Hoque MZ, Ahmad I. Latest Developed Strategies to Minimize the Off-Target Effects in CRISPR-Cas-Mediated Genome Editing. Cells. 2020;9(7):1608.
99. Hannah R, Beck M, Moravec R, Riss T. CellTiter-Glo™ luminescent cell viability assay: A sensitive and rapid method for determining cell viability. Promega Cell Notes. 2001;2.
100. Matthews J, Gustafsson JA. Estrogen receptor and aryl hydrocarbon receptor signaling pathways. Nucl Recept Signal. 2006;4:e016.
101. Wang K, Li Y, Jiang Y-Z, Dai C-F, Patankar MS, Song J-S, et al. An endogenous aryl hydrocarbon receptor ligand inhibits proliferation and migration of human ovarian cancer cells. Cancer letters. 2013;340(1):63-71.
102. Yin J, Sheng B, Qiu Y, Yang K, Xiao W, Yang H. Role of AhR in positive regulation of cell proliferation and survival. Cell Prolif. 2016;49(5):554-60.
103. Saito R, Miki Y, Hata S, Takagi K, Iida S, Oba Y, et al. Aryl hydrocarbon receptor in breast cancer—a newly defined prognostic marker. Horm Cancer. 2014;5(1):11-21.
104. Salisbury TB, Morris GZ, Tomblin JK, Chaudhry AR, Cook CR, Santanam N. Aryl hydrocarbon receptor ligands inhibit igf-ii and adipokine stimulated breast cancer cell proliferation. ISRN Endocrinol. 2013;2013:104850.
105. Dohr O, Vogel C, Abel J. Different Response of 2,3,7,8-Tetrachlorodibenzo-p-dioxin (TCDD)-Sensitive Genes in Human Breast Cancer MCF-7 and MDA-MB 231 Cells. Archives of Biochemistry and Biophysics. 1995;321(2):405-12.
106. Chang TKH, Chen J, Lee WBK. Differential Inhibition and Inactivation of Human CYP1 Enzymes bytrans-Resveratrol: Evidence for Mechanism-Based Inactivation of CYP1A2. Journal of Pharmacology and Experimental Therapeutics. 2001;299(3):874.
107. Staub RE, Onisko B, Bjeldanes LF. Fate of 3,3‘-Diindolylmethane in Cultured MCF-7 Human Breast Cancer Cells. Chemical Research in Toxicology. 2006;19(3):436-42.
108. Pondugula SR, Flannery PC, Abbott KL, Coleman ES, Mani S, Samuel T, et al. Diindolylmethane, a naturally occurring compound, induces CYP3A4 and MDR1 gene expression by activating human PXR. Toxicol Lett. 2015;232(3):580-9.
109. Guthrie AR, Chow HHS, Martinez JA. Effects of resveratrol on drug- and carcinogen-metabolizing enzymes, implications for cancer prevention. Pharmacology Research & Perspectives. 2017;5(1):e00294.
110. Hong SP, Choi DH, Choi JS. Effects of resveratrol on the pharmacokinetics of diltiazem and its major metabolite, desacetyldiltiazem, in rats. Cardiovasc Ther. 2008;26(4):269-75.
111. Choi JS, Choi BC, Kang KW. Effect of resveratrol on the pharmacokinetics of oral and intravenous nicardipine in rats: possible role of P-glycoprotein inhibition by resveratrol. Pharmazie. 2009;64(1):49-52.
112. Bedada SK, Nearati P. Effect of resveratrol on the pharmacokinetics of carbamazepine in healthy human volunteers. Phytother Res. 2015;29(5):701-6.
113. Chow HH, Garland LL, Hsu CH, Vining DR, Chew WM, Miller JA, et al. Resveratrol modulates drug- and carcinogen-metabolizing enzymes in a healthy volunteer study. Cancer prevention research (Philadelphia, Pa). 2010;3(9):1168-75.
114. Guthrie AR, Chow HHS, Martinez JA. Effects of resveratrol on drug- and carcinogen-metabolizing enzymes, implications for cancer prevention. Pharmacology research & perspectives. 2017;5(1):e00294-e.
115. Uno S, Dalton TP, Derkenne S, Curran CP, Miller ML, Shertzer HG, et al. Oral Exposure to Benzo[a]pyrene in the Mouse: Detoxication by

Inducible Cytochrome P450 Is More Important Than Metabolic Activation. Molecular Pharmacology. 2004;65(5):1225.
116. Chun YJ, Kim MY, Guengerich FP. Resveratrol Is a Selective Human Cytochrome P450 1A1 Inhibitor. Biochemical and Biophysical Research Communications. 1999;262(1):20-4.
117. Powell JB, Goode GD, Eltom SE. The Aryl Hydrocarbon Receptor: A Target for Breast Cancer Therapy. J Cancer Ther. 2013;4(7):1177-86.
118. Tomblin JK, Salisbury TB. Insulin like growth factor 2 regulation of aryl hydrocarbon receptor in MCF-7 breast cancer cells. Biochemical and Biophysical Research Communications. 2014;443(3):1092-6.
119. Spink BC, Bennett JA, Lostritto N, Cole JR, Spink DC. Expression of the aryl hydrocarbon receptor is not required for the proliferation, migration, invasion, or estrogen-dependent tumorigenesis of MCF-7 breast cancer cells. Molecular carcinogenesis. 2013;52(7):544-54.
120. Vichai V, Kirtikara K. Sulforhodamine B colorimetric assay for cytotoxicity screening. Nature protocols. 2006;1(3):1112-6.
121. Aslantürk ÖS, editor In Vitro Cytotoxicity and Cell Viability Assays: Principles, Advantages, and Disadvantages2017.
122. Vogel CFA, Lazennec G, Kado SY, Dahlem C, He Y, Castaneda A, et al. Targeting the Aryl Hydrocarbon Receptor Signaling Pathway in Breast Cancer Development. Frontiers in immunology. 2021;12:553.
123. Rodriguez M, Potter DA. CYP1A1 regulates breast cancer proliferation and survival. Mol Cancer Res. 2013;11(7):780-92.
124. Vanderlaag K, Samudio I, Burghardt R, Barhoumi R, Safe S. Inhibition of breast cancer cell growth and induction of cell death by 1,1-bis(3'-indolyl)methane (DIM) and 5,5'-dibromoDIM. Cancer Lett. 2006;236(2):198-212.
125. Chin Y-T, Hsieh M, Yang S-H, Tsai P-W, Wang s-h, Wang C-C, et al. Anti-proliferative and gene expression actions of resveratrol in breast cancer cells in vitro. Oncotarget. 2014;5.
126. Hu C, Liu Y, Teng M, Jiao K, Zhen J, Wu M, et al. Resveratrol inhibits the proliferation of estrogen receptor-positive breast cancer cells by suppressing EZH2 through the modulation of ERK1/2 signaling. Cell Biology and Toxicology. 2019;35(5):445-56.
127. Jin UH, Michelhaugh SK, Polin LA, Shrestha R, Mittal S, Safe S. Omeprazole Inhibits Glioblastoma Cell Invasion and Tumor Growth. Cancers (Basel). 2020;12(8).
128. Hanieh H, Mohafez O, Hairul-Islam VI, Alzahrani A, Bani Ismail M, Thirugnanasambantham K. Novel Aryl Hydrocarbon Receptor Agonist Suppresses Migration and Invasion of Breast Cancer Cells. PLoS One. 2016;11(12):e0167650.
129. Grimaldi G, Vagaska B, Ievglevskyi O, Kondratskaya E, Glover JC, Matthews J. Loss of Tiparp Results in Aberrant Layering of the Cerebral Cortex. eNeuro. 2019;6(6):ENEURO.0239-19.2019.
130. Jackson D, Joshi A, Elferink C. Ah Receptor Pathway Intricacies; Signaling Through Diverse Protein Partners and DNA-Motifs. Toxicol Res. 2015;4.
131. Ho J-N, Jun W, Choue R, Lee J. I3C and ICZ inhibit migration by suppressing the EMT process and FAK expression in breast cancer cells. Mol Med Rep. 2013;7(2):384-8.

9 Appendix 1

Complete lists of chemicals, equipment and software programs used

Table 1 Chemicals and biological reagents

Name	**Company**	**Catalog number #**
1X RIPA buffer	Cell Signaling Technology, Danverse, MA, USA	9806S
2,3,7,8-tetrachlorodibenzo-p-dioxin (TCDD, dioxin)	AccuStandard (New Heaven, CT, USA	D-404S
2-Mercaptoethanol	Sigma-Aldrich, St. Louis, MO, USA	M3148-100ML
2X Roche cOmplete protease inhibitor cocktail Tablets	Roche Diagnostics, Mannheim, Germany	11836145001
3,3'-Diindolylmethane (DIM)	Sigma-Aldrich, St. Louis, MO, USA	D9568-5G
4X Laemmli Sample Buffer	BioRad, Hercules, CA, USA	1610747
6X Purple Loading Dye	New England Biolabs, Ipswich, MA, USA	B7024S
AHR forward primer, 5'	Sigma-Aldrich, St. Louis, MO, USA	5'-CACTGTCCCGAGAGGACG-3'
AHR reverse primer, 3'	Sigma-Aldrich, St. Louis, MO, USA	5'-GGGAATGGACCTAATCCCAG-3'
Anti-actin, primary antibody	Sigma-Aldrich, St. Louis, MO, USA	A2228-200UL (lot: 099M4776V)
Anti-AHR, primary antibody	Enzo Life Sciences, Farmingdale, NY, USA	bml-sa210-0100 (lot: 04011942)
Anti-mouse, secondary antibody	Cell Signaling Technology, Danverse, MA, USA	7076S (lot: 35)
Anti-rabbit, secondary antibody	Cell Signaling Technology, Danverse, MA, USA	7074S (lot: 29)
Aurum™ Total RNA isolation kit	BioRad, Hercules, CA, USA	7326820

CellTiter-Glo® Luminescent Cell Viability Assay	Promega, Madison, WI, USA	G7572
CutSmart® Buffer	New England Biolabs, Ipswich, MA, USA	B7204S
Dimethyl sulfoxide (DMSO)	Sigma-Aldrich, St. Louis, MO, USA	D2650-100ML
Dithiothreitol (DTT)	Thermo Fisher Scientific, Waltham, MA, USA	P2325
Dulbecco's Modified Eagle's Medium (DMEM), 1,0 g/l glucose	Lonza, Walkersville, MD, USA	12-707F
EcoRI-HF®	New England Biolabs, Ipswich, MA, USA	R3101L
Fetal Bovine Serum (FBS)	Sigma-Aldrich, St. Louis, MO, USA	F7524
GC-RICH PCR System	Sigma-Aldrich, St. Louis, MO, USA	12140306001
GenElute™ Mammalian Genomic DNA Miniprep Kits	Sigma-Aldrich, St. Louis, MO, USA	G1N70-1KT
GeneRuler 1 kb Plus DNA Ladder	Thermo Fisher Scientific, Waltham, MA, USA	SM1333
High-Capacity cDNA Reverse Transcription Kit	Applied Biosystems, Foster City, CA, USA	4368814
Kanamycin sulfate, from Streptomyces kanamyceticus	Sigma-Aldrich, St. Louis, MO, USA	K4000-25G
L-glutamine	Sigma-Aldrich, St. Louis, MO, USA	G7513-100ML
Lipofectamine™ 2000 Transfection Reagent	Invitrogen, Carlsbad, CA, USA	11668030
M13 reverse primer	Sigma-Aldrich, St. Louis, MO, USA	5'-CAGGAAACAGCTATGAC-3'
MCF7	ATCC, Manassas, VA, USA	ATCC®HTB-22™

MDA-MB-231	ATCC, Manassas, VA, USA	ATCC®HTB-26™
MDA-MB-468	ATCC, Manassas, VA, USA	ATCC®HTB-132™
NEB® 5-alpha Competent E. coli (High Efficiency)	New England Biolabs, Ipswich, MA, USA	C2987H
NEBuffer™ 2	New England Biolabs, Ipswich, MA, USA	B7002S
NucleoSpin Plasmid, Mini kit for plasmid DNA	Macherey-Nagel, Düren, Germany	740588.250
NucleoSpin® Gel and PCR Clean-up kit	Macherey-Nagel, Düren, Germany	740609.250
Opti-MEM™ Reduced Serum Medium	Thermo Fisher Scientific, Waltham, MA, USA	31985062
pCR™2.1 Vector	Invitrogen, Carlsbad, CA, USA	K202020
Pencillin-Streptomycin	Sigma-Aldrich, St. Louis, MO, USA	P4458-100ML
pGEM®-T Easy Vector Systems	Promega, Madison, WI, USA	A1360
Pierce™ BCA Protein Assay Kit	Thermo Fisher Scientific, Waltham, MA, USA	23225
Pierce™ Bovine Serum Albumin Standard (BSA), 2 mg/ml	Thermo Fisher Scientific, Waltham, MA, USA	23210
RBN-2397	MedChemExpress, Monmouth Junction, NJ, USA	HY-136174
Resorufin ethyl ether, ETX	Sigma-Aldrich, St. Louis, MO, USA	46121
Resveratrol	Sigma-Aldrich, St. Louis, MO, USA	R5010-100MG
SeaKem® LE Agarose	Lonza, Walkersville, MD, USA	50004
Skim Milk Powder	Sigma-Aldrich, St. Louis, MO, USA	70166-500G
Sso Advanced™ Universal SYBR® Green Supermix	BioRad, Hercules, CA, USA	1725271
SuperSignal West Pico PLUS	Thermo Fisher Scientific, Waltham, MA, USA	34577

chemiluminescent Substrate		
SuperSignal™ West Dura Extended Duration Substrate	Thermo Fisher Scientific, Waltham, MA, USA	34076
SuperSignal™ West Femto Maximum Sensitivity Substrate	Thermo Fisher Scientific, Waltham, MA, USA	34095
T7 endonuclease I	New England Biolabs, Ipswich, MA, USA	M0302L
Trypsin	Sigma-Aldrich, St. Louis, MO, USA	T3924-100ML
Water	Sigma-Aldrich, St. Louis, MO, USA	W4502-1L

Table 2 Equipment used

Name	**Producer**	**Catalog number**
CFX96 Touch™ Real-Time PCR Detection System	BioRad, Hercules, CA, USA	1855195
ChemiDoc™ Touch Imaging System	BioRad, Hercules, CA, USA	1708370
Corning® 96-well plates, white/clear bottom polystyrene microplate	Corning Incorporated, Kennebunk, ME, USA	3610
Criterion™ TGX™ Precast Gels	BioRad, Hercules, CA, USA	5671033, 5671034
Gel Doc™ XR+ Gel Documentation System	BioRad, Hercules, CA, USA	1708195
Immobilon-P polyvinylidene fluoride (PVDF) membrane	MerckMillipore, Burlington, MA, USA	IPVH00010
pH meter pH 1000 L	VWR, Radnor, PA, USA	ECN: 662-1422
PowerPac™ Basic Power Supply	BioRad, Hercules, CA, USA	1645050
Synergy H1 Hybrid Multi-Mode Reader	BioTek, Winooski, VT, USA	111-120-533
Veriti™ 96-Well Thermal Cycler	Applied Biosystems, Foster City, CA, USA	**4375786**
Zeiss Axiocam 305 mono	Zeiss, Oberkochen, Germany	Zeiss Axiocam 305 mono

Table 3 Software programs used

Name	**Producer**	**Version/Link for download**
Graphpad Prism	San Diego, CA, USA	8.3.0
ImageJ	Wayne Rasband and contributors, National Institutes of Health, USA	1.53e https://imagej.nih.gov/ij/index.html
ImageJ Wound Healing Size Tool plugin	Suarez-Arnedo et al., 2020, Department of Biomedical Engineering, Universidad de los Andes, Bogotá, Colombia	https://github.com/AlejandraArnedo/Wound-healing-size-tool/wiki
Zeiss Zen 2	Zeiss Oberkochen, Germany	2.6 (blue edition)